

1 A new inventory of High Mountain Asia surging glaciers derived from 2 multiple elevation datasets since the 1970s

3 Lei Guo¹, Jia Li¹, Amaury Dehecq², Zhiwei Li¹, Xin Li³, Jianjun Zhu¹

4 ¹School of Geo-science and Info-physics, Central South University, Changsha, 410083, China.

5 ²Univ. Grenoble Alpes, IRD, CNRS, Grenoble INP, IGE, Grenoble, 38000, France.

6 ³Institute of Tibetan Plateau Research, Chinese Academy of Sciences, Beijing, 100101, China.

7

8 *Correspondence to:* Jia Li (lijia20050710@csu.edu.cn)

9 **Abstract.** Glacier surging is an unusual instability of ice flow and ~~complete~~ inventories of surging glaciers are important for
10 regional glacier mass balance studies and glacier dynamic studies. Glacier ~~surge events~~ surges in High Mountain Asia (HMA)
11 ~~are have been~~ widely reported. However, the completeness of ~~present~~ available inventories of HMA surging glaciers is
12 ~~constrained~~ hampered by the insufficient spatial and temporal coverage of glacier change observations, or by the limitations of
13 the identification methods. In this study, we established a new inventory of HMA surging glaciers based on ~~the~~ glacier surface
14 elevation changes and morphological changes over four decades. ~~Four types of~~ Three elevation change datasets based on four
15 elevation sources (the KH-9 DEM, NASA DEM, COP30 DEM, and HMA DEM), ~~three elevation change datasets,~~ and long-
16 term Landsat satellite image series were utilized to assess the presence of typical surge features over two time periods (1970s-
17 2000 and 2000-2020). A total of 890 surging and 336 probably or possibly surging glaciers were identified in HMA. Compared
18 to the most recent inventory of surging glaciers in HMA, our inventory incorporated 253 previously unidentified surging
19 glaciers. The number and area of surging glaciers accounted for ~2.49% (excluding glaciers smaller than 0.4 km²) and ~16.59%
20 of the total glacier number and glacier area in HMA, respectively. Glacier surges were found in 21 of the 22 subregions of
21 HMA (except for the Dzhungarsky Alatau); however, the density of surging glaciers is highly uneven. ~~They are~~
22 ~~common~~ Glacier surges occur frequently in the northwestern subregions (e.g., Pamir and Karakoram), but ~~searee~~ less often in
23 the peripheral subregions. The inventory further ~~confirmed~~ shows that surge activity is more likely to occur for glaciers with a
24 larger area, longer length, and wider elevation range. Among glaciers with similar areas, the surging ones usually have steeper
25 slopes than non-surging ones. ~~Besides, we found a potential relationship between surging glacier concentration and regional~~
26 ~~glacier mass balance. The subregions with slightly negative or positive mass balance hold large clusters of surging glaciers,~~
27 ~~while those with severe mass loss hold very few surging glaciers.~~ The inventory and elevation change products of identified
28 surging glaciers are available at: <https://doi.org/10.5281/zenodo.79612077950838> (Guo et al., 2022).

29 **Key words:** High Mountain Asia, Surging glacier inventory, elevation change, KH-9, Digital Elevation Model (DEM)

30 1 Introduction

31 A surge is a glacier instability that translates into an abnormally fast flow over a period of a few months to years (Cogley et
32 al., 2011). A surging glacier exhibits an active phase (surge) and a quiescent phase that may occur at quasi-periodic intervals
33 (Jiskoot, 2011). During a glacier's surging phase, a large volume of ice mass is transported downstream at a higher-than-
34 average speed. In the quiescent phase, a glacier returns to a slow-moving state, and gradually regains mass in ~~upper reaches~~ the
35 reservoir zone.

36 Previous studies pointed out that surge-type glaciers only represent ~1% of total glaciers (Jiskoot, 2011; Sevestre and Benn,
37 2015). However, glacier surges are far more than an occasional behavior in some specific regions, such as the Alaska-Yukon
38 (Clarke et al., 1986), Svalbard (Jiskoot et al., 2000; Farnsworth et al., 2016), and Karakoram-Pamir (Bhambri et al., 2017;
39 Goerlich et al., 2020; Guillet et al., 2022). Glaciers in these regions have experienced heterogeneous mass loss in the past

40 decades (Hugonnet et al., 2021). ~~Understanding~~ how glacier surge activities impact the regional mass balance ~~needs further~~
41 ~~investigation and~~ requires ~~to identify first~~ the ~~glacier surges firstly~~ ~~identification of surging glaciers~~. In recent years, substantial
42 efforts have been made to understand the mechanisms of glacier surges, including ~~the models that account for~~ hydrological-
43 ~~controls~~ (Kamb, 1987; Fowler, 1987), thermal-~~controls~~ (Fowler et al., 2001; Murray et al., 2003), environmental factors
44 (Hewitt, 2007; Van Wyk de Vries et al., 2022), friction state (Thøgersen et al., 2019; Beaud et al., 2021), and ~~the unified~~
45 enthalpy (Sevestre and Benn, 2015; Benn et al., 2019) ~~balance model~~. These theories require comprehensive validations by
46 conducting detailed analysis on various glacier samples. To support related investigations, the distribution of surging glaciers
47 is needed as a starting point.

48 Generally, a surging glacier ~~could exhibit either~~ ~~exhibits~~ one or several ~~drastic~~ ~~of the following~~ changes, ~~including~~: extreme
49 ~~speed-up~~ ~~increase in flow velocity~~ (by a factor of 10~1000 compared to the usual flow of non-surging glaciers),
50 ~~distinct~~ ~~contrasting~~ elevation change pattern; ~~(e.g. thickening in lower reaches and thinning in upper reaches)~~, rapid terminus
51 advance, and surface morphological changes (deformed ~~medial~~ or looped ~~medial~~ moraines, ~~erevasses~~, ~~shear~~ ~~intense~~ ~~crevassing~~
52 ~~or shearing at the~~ margins, ~~etc.~~) (Jiskoot, 2011). The identification of surging glaciers can be implemented based on the
53 observation of ~~the above~~ ~~these~~ changes, e.g., ~~by studying~~ glacier surface morphology (Clarke et al., 1986; Paul, 2015;
54 Farnsworth et al., 2016), terminus position (Copland et al., 2011; Vale et al., 2021), glacier motion (Quincey et al., 2011), or
55 morphological-related indicators (e.g., normalized backscatter difference (Leclercq et al., 2021) ~~)).~~). A surge-type glacier,
56 which refers to a glacier that possibly surged prior to the observation period, is generally identified by indirect morphological
57 evidence (without observed changes) (Goerlich et al., 2020). The visual interpretation of glacier surface morphological changes
58 is less calculative, but ~~fraught with uncertainty~~ ~~is prone to uncertainties~~ due to the snow cover or the absence of supraglacial
59 moraine deformation (Jacquemart and Cicoira, 2022). To recognize sudden changes in glacier motion, a long-term flow
60 velocity time series is needed (Yasuda and Furuya, 2015; Round et al., 2017). Since the quiescent phase may last for decades
61 and the image sources for estimating ~~the~~ flow velocity are limited, the strong changes in glacier motion ~~associated with the~~
62 ~~surge~~ might be missed. In contrast, the recognition of a specific surface elevation change pattern ~~is can be~~ a more reliable way
63 to identify surging glaciers, as it ~~will be~~ ~~can remain~~ visible for many years before and after a surge (Bolch et al., 2017; Zhou et
64 al., 2018). ~~Accordingly, its source~~ ~~datasets~~ ~~Besides, digital elevation models~~ (DEMs) can satisfy the required spatio-temporal
65 coverage with comparatively fewer datasets. By combining observations of ~~multiple~~ ~~changes in glacier surface elevation, flow~~
66 ~~velocity, and morphological~~ features, the identification of surging glaciers could be more efficient and complete (Mukherjee
67 et al., 2017; Goerlich et al., 2020; Guillet et al., 2022). ~~However,~~ When conducting such studies on a large spatial scale or a
68 long temporal scale, one should select the least time-consuming but most effective identification method. In that case, ~~it's ideal~~
69 ~~to take the long term~~ ~~datasets of~~ elevation change ~~as a criterion and to combine~~ ~~covering many decades can be helpful,~~
70 ~~especially if~~ this information ~~is combined~~ with other observations ~~if possible~~ ~~such as flow velocity and morphological changes~~
71 (Guillet et al., 2022).

72 ~~Except for the polar regions,~~ High Mountain Asia (HMA) is the most densely glacierized region in the world; ~~outside the polar~~
73 ~~regions~~. Within ~~the HMA range~~, several subregions are ~~famous~~ ~~well known~~ for the concentration of surging glaciers as well as
74 the differing glacier mass balance ~~in contrast to the common thinning in other glacierized regions~~ (Hewitt, 2005; Gardelle et
75 al., 2013; Farinotti et al., 2020). ~~The~~ Inventories of surging or surge-like glaciers have been established for some subregions
76 like the Karakoram (Bhambri et al., 2017), West-Kunlun (Yasuda and Furuya, 2015), Pamir (Goerlich et al., 2020) and Tien
77 Shan (Mukherjee et al., 2017; Zhou et al., 2021). Sevestre and Benn (2015) presented the first global inventory of surging
78 glaciers by reanalyzing historical reports from 1861 to 2013. However, it was compiled from various data sources (publications,
79 reports, etc.) with inconsistent spatio-temporal coverage, which makes it difficult to ensure accuracy and completeness. Vale
80 et al. (2021) identified 137 surging glaciers across HMA by detecting surge-induced terminus change and morphological
81 changes from Landsat images ~~from~~ ~~obtained between~~ 1987 ~~to~~ ~~and~~ 2019. ~~The~~ ~~is~~ number ~~is obviously underestimated, because it,~~
82 ~~however,~~ is smaller than the numbers of previous subregional inventories (Bhambri et al., 2017; Goerlich et al., 2020),

83 ~~i.e. because~~ not all glaciers that surge do also advance. Guillet et al. (2022) presented a new surging glacier inventory of HMA
84 by identifying multiple glacier change features. In total, 666 surging glaciers were identified across HMA. However, the glacier
85 change observation period is shorter than two decades (2000-2018), and therefore some surging glaciers with relatively long-
86 repetition cycles may be missed.

87 In this study, we aimed to build a new inventory to include more surging glaciers within HMA based on glacier surface
88 elevation changes observations over four decades. A workflow was developed to obtain the historical glacier surface elevation
89 change from multiple DEMs, including the KH-9 DEM (1970s), NASA DEM (2000), COP30 DEM (2011-2014), HMA DEM
90 (2002-late 2016), and previously published elevation change datasets. The preliminary identified surging glaciers were divided
91 into three classes of confidence in surge detection. After that, ~~the is~~ elevation-~~change~~ based inventory was further completed
92 and corrected by ~~the identification of identifying~~ morphological changes in a ~~long-term~~ time series of optical Landsat images
93 ~~(between 1986- and 2021)~~. Based on the present inventory, the distribution and geometric characteristics of surging glaciers
94 within HMA were statistically analyzed, in order to demonstrate their spatial heterogeneity and geometrical difference from
95 the normal glaciers.

96 2 Study region

97 High Mountain Asia consists of the Qinghai-Tibet Plateau and its surrounding regions, including the Karakoram, Pamir,
98 Himalayas, and Tien Shan. According to the updated Glacier Area Mapping for Discharge from the Asian Mountains
99 (GAMDAM2) glacier inventory, HMA hosts 131819 glaciers, covering a total area of ~99817 km² (Sakai, 2019). The Hindu
100 Kush Himalayan Monitoring and Assessment Programme (HiMAP) divided HMA into 22 subregions (Fig-~~ure~~ 4) (Bolch et al.,
101 2019). Different subregions are influenced by different climate regimes, such as the South Asia monsoon, the East Asia
102 monsoons, and the westerlies (Bolch et al., 2012; Maussion et al., 2014). Glacier elevation changes across HMA were found
103 to be heterogeneous in the past decades (Gardelle et al., 2013; Brun et al., 2017; Shean et al., 2020). In particular, glaciers in
104 the Pamir-Karakoram-West Kunlun region had slightly positive or close to zero changes (Hewitt, 2005; Zhou et al., 2017;
105 Farinotti et al., 2020), while those in the Eastern Himalayas, Nyainqentanglha and Hengduan Shan mountain ranges
106 experienced substantial ice loss (Maurer et al., 2019).

107 3 Datasets

108 3.1 Elevation Data

109 The NASA DEM is mainly reprocessed from ~~the~~ C-band SRTM (Shuttle Radar Topography Mission) images data. Among the
110 current global DEMs, the NASA DEM has the shortest source data acquisition period (~11/02/2000~22/02/2000) (Farr et al.,
111 2007). Based on an improved production flow, the NASA DEM has a better performance than the earlier SRTM void-free
112 product in most regions (Crippen et al., 2016). The NASA DEM serves as the reference elevation source because its acquisition
113 time, 2000, is suitable to divide the elevation change observations into periods before and after the beginning of the 21st century
114 with a moderate time span (one or two decades). Each tile of the product has an extent of 1°× 1° and a pixel spacing of 1 arc-
115 second (see Fig-~~ure~~ 1a). In total, 313 tiles were downloaded from NASA LP DAAC
116 (https://e4ftl01.cr.usgs.gov/MEASURES/NASADEM_HGT.001/).

117 Another global DEM we ~~utilized~~ used is the newly released Copernicus DEM GLO-30-DGED (i.e., COP30 DEM). The COP30
118 DEM was edited from the ~~delicate~~ WorldDEM™, which was generated based on the TanDEM-X mission. The global RMSE
119 of the COP30 DEM is ±1.68 m (AIRBUS, 2020). Several studies have pointed out that this DEM is the most reliable open-
120 access DEM to date (Purinton and Bookhagen, 2021; Guth and Geoffroy, 2021). The source images of the COP30 DEM were
121 mostly acquired between 2011 and 2014, and therefore the COP30 DEM is suitable for representing the surface elevation in

122 the 2010s. Like the NASA DEM, the COP30 DEM has a pixel spacing of 1 arcsecond. Each tile of the product has an extent
123 of $1^{\circ} \times 1^{\circ}$. In total, 313 tiles were downloaded through ESA Panda (<https://panda.copernicus.eu/web/cds-catalogue/panda>).
124 The High Mountain Asia 8-meter DEM (HMA DEM) was also utilized in this study. The HMA DEM was generated from
125 very high-resolution commercial optical satellite stereo images, including WorldView-1/2/3, GeoEye-1, and Quickbird-2
126 (Shean et al., 2020), through an automated photogrammetry workflow that is integrated with multiple error-control processes
127 (Shean et al., 2016). This DEM was originally produced for the mass balance estimation of HMA glaciers, so it covered most
128 of the glacierized regions in HMA. In total, 3598 DEM tiles were downloaded from the National Snow and Ice Data Center
129 (https://nsidc.org/data/HMA_DEM8m_MOS/versions/1). About 95% of ~~them~~the underlying stereo images were acquired
130 between 2010 and 2016 (Fig-[ure](#) 1b). Due to the data voids and inconsistent acquisition time, the HMA DEM was taken as a
131 supplementary elevation source to increase the observations data coverage in the 2010s.
132 The Hexagon KeyHole-9 (KH-9) imagery was acquired in the 1970s. It is one of the earliest near-global satellite stereo image
133 sources. The KH-9 imagery is characterized by a spatial resolution of 6-9 m, a wide coverage (130 km x 260 km), and a 70%
134 forward overlap (Surazakov and Aizen, 2010). Many studies have utilized this imagery to estimate historical glacier surface
135 elevation (Holzer et al., 2015; Zhou et al., 2017; Maurer et al., 2019). The KH-9 DEMs used in this study were generated
136 through the automated ASPy pipeline (Dehecq et al., 2020). The methodology, validated in the European Alps and Alaska,
137 achieved a vertical accuracy of ~5m (68% confidence level). For more details on the method of KH-9 DEM generation,
138 please~~we~~ refer to Dehecq et al. (2020). In total, 238 DEMs with a spatial resolution of 48 m were generated from the KH-9
139 images acquired between 1973 and 1980 (see Fig-[ure](#) 1c). The KH-9 DEMs were utilized to represent the glacier surface
140 elevation in the 1970s.
141 Several newly published elevation change datasets were also collected to ~~include~~document the ~~most recent~~ surges that occurred
142 between 2000 and 2020 (Brun et al., 2017; Shean et al., 2020; Hugonnet et al., 2021). We mainly used the elevation change
143 results presented by Hugonnet et al. (2021) to extend the observation period to 2020, which has a spatial resolution of 100 m
144 and a temporal interval of 5 years. Through the inter-comparison of the multiple elevation change results, ~~the~~ gross errors or
145 false signals in ~~the~~ elevation change patterns from either our study or previously published results could be easily detected and
146 removed.

147 3.2 Optical Satellite Images

148 ~~In order~~-To assist in the identification of surging glaciers, we also ~~identified~~analyzed morphological changes associated with
149 surges in multi-temporal optical satellite images. We mainly relied on the 1986-2021 Landsat imagery to capture
150 morphological changes. We acknowledge that due to the 30 m spatial resolution, not all details of ~~a changed~~ glacier surfaces
151 are visible. We downloaded from the USGS (<https://earthexplorer.usgs.gov>) the false-color composited LandsatLook images
152 with ~~30m~~30 m resolution (geo-referenced) that have good brightness contrast over snow/ice areas ~~from the USGS (-)~~. The
153 Only images ~~were pre-selected to satisfy the requirement of~~ with less than 10% cloud cover (<10%) were selected. In total,
154 7843 LandsatLook images ~~in~~from 148 frames were used (see Fig-[ure](#) 1d). We also utilized the very high-resolution (VHR)
155 images~~basemaps~~ (Google/ESRI/Bing, etc.) as complements for surging feature identification. The fine resolution of these
156 images allows us to visually check the possible morphological features caused by past surges.

157 3.3 Glacier inventory

158 In this study, we used the GAMDAM2 glacier inventory (Sakai, 2019) as a template for the inventory of surging glaciers,
159 rather than the Randolph Glacier Inventory V6.0 (RGI6.0) (RGI Consortium, 2017). The GAMDAM glacier inventory has
160 included many small glaciers that are missed in RGI6.0, and provides a more accurate glacier extent by also excluding rock
161 ~~outcrop~~rocks~~outcrops~~, seasonal snow, and shaded areas (Nuimura et al., 2015). Since the GAMDAM2 inventory only contains
162 the glacier polygon vectors, we calculated the geometric and topographic attributes for each glacier in a way similar to that of

163 RGI6.0. The maximum glacier ~~centreline~~centerline was calculated through the Open Global Glacier Model (OGGM)
164 (Maussion et al., 2019). The attributes were used to ~~interpret~~analyze the geometric characteristics of surging glaciers.

165 4 Methodology

166 4.1 Estimation of glacier surface elevation change

167 The four kinds of DEMs have different coordinate references, vertical references, and data formats. Firstly, all DEMs were
168 converted to float GeoTiff format. For datasets with quality files (the NASA DEM and the COP30 DEM), the DEMs were
169 preprocessed to mask out the pixels of low quality. ~~The poor~~ Pixels in the COP30 DEM ~~tile were determined through the~~
170 ~~attached with~~ height error ~~map (with values~~ larger than 2.5 m) ~~and or within the attached~~ water body ~~map (with values not~~
171 ~~equal to zero)~~mask were excluded. The NASA DEM was directly masked with the attached water mask file. Subsequently,
172 the coordinate system, map projection, and vertical reference of all DEMs tiles were ~~unified~~set as the WGS84 coordinate
173 system, ~~HMA~~an Albers Equal Area projection ~~customized for HMA regions~~ (Shean et al., 2020), and ~~the~~ WGS84 ellipsoid.
174 ~~The reprojection was performed using cubic resampling~~. The glacier surface elevation changes during 2000-2010s were
175 derived by subtracting the NASA DEM from the COP30 DEM and HMA DEM, and those during 1970s-2000 were derived
176 by subtracting the KH-9 DEM from the NASA DEM.

177 An automated DEM differencing workflow for large-scale glacier surface elevation change estimation was developed based
178 on the *demcoreg* package presented by Shean et al. (2019). The workflow ~~integrated~~s multiple DEM co-registration approaches,
179 such as ~~the~~a polynomial fit of tilt error, and other adaptive outlier removal approaches that were operated based on ~~the~~
180 observations over stable regions. Hence, a mask that excluded the water bodies and glacierized regions was generated in
181 advance. Before differencing, the two DEMs need to be co-registered, because a small geolocation shift can result in
182 considerable elevation change errors in high-mountain regions. The efficient analytical DEM co-registration method presented
183 by Nuth and Kääb (2011) was used to eliminate ~~the~~a relative geolocation shift (horizontal and vertical) between DEMs. This
184 method assumes the geolocation shift vectors of all DEM pixels are identical. However, for the global DEM products like the
185 NASA DEM and the COP30 DEM, a DEM tile was usually merged from multiple DEM patches, and the geolocation shift
186 vectors at different parts of the DEM tile may be different. In view of this problem, we developed a block-wise version of the
187 analytical DEM co-registration method to reduce the impacts of ~~the non-uniform~~ geolocation ~~accuracy anisotropy~~errors of a
188 DEM tile. Each DEM tile was divided into $m \times n$ blocks, and ~~the~~ DEM shifts were estimated for each block. Then, the $m \times n$
189 groups of shift parameters were merged into one group of shift parameters through a cubic interpolation. Technically, the
190 estimated shift parameters become increasingly representative as the block size decreases. However, the fitting of shift
191 parameters requires a certain number of samples. The final block size was set to 300×300 pixels to reach the best balance
192 between the representativeness and estimation accuracy of the shift parameters. Besides, we found that the block-wise co-
193 registration method could result in wrong fitting of shift parameters over flat regions. To deal with this, a threshold of mean
194 slope (10°) was set to classify the DEMs into the flat and the hilly ~~category~~terrain, and the original global co-registration
195 method (Nuth and Kääb, 2011) was applied to the flat ~~ones~~areas.

196 Due to the residual orbital error of satellite images, the elevation difference (dH) maps often showed planimetric trends. This
197 type of systematic error was ~~fitted as a universal surface trend using~~corrected by subtracting from the elevation change a
198 quadratic polynomial model ~~based on which was fitted to~~ the observations in ~~assumed~~ stable regions, ~~and then was removed~~
199 ~~from the elevation difference tile~~ (Li et al., 2017). Besides, due to the jitter of the SAR antenna and optical mapping camera,
200 the elevation difference maps often showed stripes (i.e., band-like artifacts) (Yamazaki et al., 2017). To eliminate the stripes,
201 the elevation difference map was converted to the frequency domain through a Fast-Fourier-Transform method. Since the
202 cyclic values have a high frequency in the power spectral density map, a threshold of frequency was set to separate the stripes
203 components from the normal elevation differences. The de-stripping was completed after the backward transformation. Finally,

204 ~~pixels for which the outliers of elevation difference maps was larger than three times the standard deviation of all pixels were~~
205 ~~reduced through the 3-sigma threshold criterion considered as outliers and removed.~~

206 The radar penetration into ~~glacier surfaces snow and ice~~ can result in ~~elevation~~ biases of ~~elevation change estimation, which~~
207 ~~could be several to dozenstens~~ of meters, ~~and potentially lead to false values over glaciers.~~ We adopted a two-step procedure
208 to reduce the radar penetration bias in the final elevation change results. First, we used the DEM differencing workflow
209 mentioned above to subtract the NASA DEM from the SRTM-X DEM. The elevation differences over glacierized area were
210 regarded as the penetration difference between X-bands and C-bands. Secondly, we fitted a ~~3rd~~-polynomial function ~~of degree~~
211 ~~three to the relationship~~ between ~~the glacial dH elevation difference~~ and altitude, which ~~was deemed as accounts for the fact~~
212 ~~that penetration depth increases at higher altitude relationship. Then, the, in drier snow and ice conditions. The estimated~~
213 radar penetration biases were removed from the COP30 DEM ~~related results by taking the glacier elevation as input for the~~
214 ~~function to NASA DEM difference over glaciers.~~ For the dH results calculated by differencing the NASA DEM and optical
215 DEMs (e.g. the HMA and KH-9 DEM), the penetration difference of X- and C- bands was multiplied by 2 to ~~represent account~~
216 ~~for the absolute fact that the~~ penetration depth of C-band ~~is approximately twice that of X-band in dry snow~~ (Rott et al., 1993;
217 Abdel Jaber et al., 2019; Fan et al., 2022) and then ~~removed subtracted~~ from the related results.

218 ~~Finally, three elevation change maps were calculated: the COP30 DEM – NASA DEM, the HMA DEM – NASA DEM, and~~
219 ~~the NASA DEM – KH 9 DEM. The first two elevation change maps were combined with the three elevation change datasets~~
220 ~~for surging glacier identification during the period 2000–2020, and the last one during the period 1970s–2000.~~ In total, our
221 elevation change observations covered ~92% of the total glacier area within HMA in 2000–2020, and ~77% in 1970s–2000.
222 Gaps in observations were mainly due to: 1) data voids and incomplete coverage of the original DEMs tile, which was the
223 main cause for the KH-9 DEMs and HMA DEM related results; 2) gross error removal during the elevation change calculations,
224 which led to the scattered holes in the COP30 DEM related results.

225 4.2 Surging glacier identification

226 The identification of surging glaciers in this study was divided into three steps. First, we generated a raw inventory of surging
227 glaciers through the qualitative interpretation of multi-temporal elevation changes. Then, the visual identification of
228 morphological changes was carried out for the identified surging and surge-like glaciers. This procedure can further confirm
229 the surges or correct the false identifications based on glacier elevation changes (Guillet et al., 2022). The identified results
230 were ~~re-~~checked ~~again~~ by careful inspection on VHR images, and by comparing ~~them~~ with existing surging glacier inventory.
231 ~~Also Besides~~, the surging tributaries were separated from the non-surging glacier trunk at this step.

232 4.2.1 Identification through elevation changes

233 ~~In general,~~ A typical glacier surge cycle can be divided into three phases (Jiskoot, 2011): 1) the build-up phase, characterized
234 by remarkable thickening in the upper reaches; 2) the active phase, characterized by remarkable thinning in the upper reaches
235 and thickening in the lower reaches; 3) the post-surge phase, characterized by strong down-wasting in the lower reaches. The
236 classical method of identifying surging glaciers is to recognize the combination of marked upper thinning and lower thickening
237 in the longitudinal direction. However, to distinguish the surging glaciers in the build-up or post-surge phase, careful
238 comparison with surrounding glaciers is required, which is difficult to be carried out with a mathematical index. In this study,
239 we established a three-class indicator to distinguish the surge possibility through the visual ~~interpretation recognition~~ of
240 ~~continuous~~ glacier elevation ~~change patterns: changes over an area larger than 0.04 km² that are higher than the thresholds~~
241 ~~listed below:~~

242 I) “verified”:

- 243 - a) obvious thickening in lower reaches (e.g., +30 m);
- 244 - b) contrasting upper-thinning (e.g., -20 m) and lower-thickening (e.g., +20 m);

- c) contrasting upper-thickening (e.g. +20 m) and lower-thinning (e.g. -30 m);
- d) severe thinning in the lower reaches (two times stronger than that of the normal glaciers, or comparable to the ablation of adjacent “verified” surging glaciers);

II) “probable”:

- **ae**) moderate upper thinning (e.g. -15m) and lower thickening (e.g. +15m);
- **bf**) only moderate thickening in the middle reaches (e.g. +15m);

III) “possible”:

- **ag**) only moderate thickening at the terminus (e.g. +15m);
- **bh**) only strong thinning in the lower reaches (one time stronger than adjacent normal glaciers).

Note that, the specific values of elevation change mentioned above were for information only. Because of the diversity in the regional elevation change patterns under different climate or topographic conditions, the thresholds may vary spatially.

The identification of surging glaciers was conducted separately in the two observation periods (1970s-2000 and 2000-2020).

The sub-inventory covering the period 1970s-2000 was generated based on the dH results of the NASA DEM – KH-9 DEM.

For the sub-inventory covering the period 2000-2020, ~~the~~ dH datasets contain the COP30 DEM – NASA_DEM, the HMA

DEM – NASA_DEM, and three previously published elevation change datasets [from Brun et al. \(2017\)](#), [Shean et al. \(2020\)](#)

[and Hugonnet et al. \(2021\)](#). Within each observation period, each glacier ~~will be~~ **was** labeled with its possibility level of surging

and elevation change pattern in the attribute table. For example, the label “I-c” means this glacier was classified as a “verified”

surging glacier because contrasting upper-thickening and lower-thinning patterns were observed in the corresponding period.

Figure 2 shows an example of surging glacier identification result.

4.2.2 Identification through morphological changes

Long-term Landsat images (acquired between 1986 and 2021) were utilized to investigate the morphological changes of the

three types of potential surging glaciers identified from elevation change. ~~With~~ **in** each Landsat ~~image~~ acquisition frame, all

Landsatlook images of different dates (acquired from 1986 to 2021) were merged into an animated time-series image. Based

on the animated image, we are able to ~~easily~~ **identify** ~~the~~ morphological changes. Due to the moderate resolution of Landsat

images, only three types of feature changes were utilized as criteria for identifying glacier surges: terminus position change,

looped moraine changes, and medial moraine changes. Similarly, we assigned a two-level index to each morphological change

to indicate our confidence in the identification, which was defined as follows:

1) terminus advance:

~~T1~~ **T1**): ~~obvious~~ **strong** terminus advancing (e.g. over 500 m);

~~T2~~ **T2**): slight terminus advancing (e.g. 0~500 m);

2) looped/medial moraine change:

~~M1~~ **M1**): fast formation/vanishment of the looped moraine, or obvious distortion of the medial moraine;

~~M2~~ **M2**): slow formation or vanishment of the looped moraine, or slight shape changes of existing looped moraine, or slight distortion of the medial moraine.

Each of the three kinds of morphological changes was individually qualified and labeled in the attribute table. [All criteria used](#)

[for identifying surging glaciers were listed in Table 1.](#)

4.2.3 Generation of surging glacier inventory

Through the above identification steps, in total five indicators were compiled to describe the changes of possible surging

glaciers. The two sub-inventories ~~of dH identified results based on elevation change maps (section 4.2.1)~~ were **first** merged

firstly following the principle of possibility, i.e., if a glacier was identified as a surging glacier in both periods but associated

with different indicators, its indicator in the final inventory was taken from the indicator having a higher possibility. The

286 possibility of indicators follows the order: “verified” > “probable” > “possible”. For example, a glacier ~~was~~ identified as a
287 “verified” surging glacier in the period 1970s-2000, and ~~was~~ identified as a “probable” surging glacier in the period 2000-
288 2010s, ~~then it was~~ quaclassified as a “verified” surging glacier. ~~After that, the merged dH indicators were~~ This intermediate
289 inventory was further ~~empa~~rged with the inventory based on morphological indicators to determine the final indicator of
290 surge possibility. The “probable” or “possible” class was changed to a class with higher possibility (e.g., from “probable” to
291 “verified”) only if an ~~“I” kind of obvious~~ morphological change was ~~found~~observed (i.e., “T1” type of terminus advancing or
292 “M1” type of looped/medial moraine change).

293 We think the advancing glaciers usually have such features: 1) only thickened in a small area at the terminus, without
294 contrasting upper thinning; 2) the advancing distance is relatively short (Lv et al., 2019, 2020; Goerlich et al., 2020). These
295 features ~~are corresponding~~correspond to the “III-ag” type of elevation change, and the “HT1” type of terminus advance.
296 Therefore, if a glacier only shows these two kinds of changes, it will be qualified as an advancing glacier, rather than a surging
297 glacier.

298 For ~~glacier complex glaciers~~, in which a tributary surged but the main trunk did not show any features of a surge, such as ~~the~~
299 Biafo ~~glacier~~, Fedchenko ~~Glacier~~, and, or Panmah glaciers (Hewitt, 2007; Goerlich et al., 2020; Bhambri et al., 2022), ~~it’s~~
300 ~~necessary to separate~~we separated the surging tributary from the trunk. A tributary will be considered as an individual surging
301 glacier ~~if it has~~in the following ~~features~~. ~~Firstly, conditions~~: the transition of contrasting elevation change is located in this
302 tributary. ~~Secondly, and~~ the mass contributed by this tributary to the glacier trunk is relatively small. ~~Then~~In that case, we
303 manually edited the outline to separate the tributary from the glacier complex. This kind of surge was also marked by the
304 attribute ~~of~~ “trib_surge”.

305 In the final step, we inspected the identified surging glaciers on VHR imagery. The inspection aimed to remove ~~the~~ wrong
306 ~~identification due to~~identifications caused by some false signals, such as the severe lower-thinning in a lake-terminating glacier
307 and remarkable surface heightening caused by nearby landslides. We also refined our inventory after careful comparison with
308 inventories presented by Guillet et al. (2022), Goerlich et al. (2020), and Bhambri et al. (2017).

309 4.3 Estimation of the uncertainty

310 ~~The reliability of surging glacier identification is directly related to the accuracy of glacier surface elevation change. Assuming~~
311 ~~the uncertainties in elevation difference are similar over glacierized and stable areas, we evaluated the uncertainties of glacier~~
312 ~~elevation difference based on elevation difference observations in stable areas, whose true values are zeros. Here we adopted~~
313 ~~the normalized median absolute deviation (NMAD) as the indicator of uncertainty of elevation difference, which is less~~
314 ~~sensitive to outliers and can be deemed as a better proxy of the standard deviation for dH in mountainous area~~ (Höhle and
315 Höhle, 2009; Li et al., 2017). ~~The NMAD is calculated as follow:~~

$$316 \text{NMAD} = 1.4826 \times \text{median}(|\Delta h_i - \text{median}(\Delta h)|) \quad (1)$$

317 ~~where Δh is the elevation difference and the subscript i denotes the index of the pixel.~~

318 ~~In this study, uncertainties in glacier elevation change are caused by uncertainties in the elevation difference and in the~~
319 ~~penetration depth. Since the penetration depth was also estimated from a DEM difference (SRTM-X DEM – NASA DEM),~~
320 ~~its uncertainty can also be evaluated through the NMAD. Assuming that these two kinds of uncertainties are uncorrelated,~~
321 ~~the uncertainty of the glacier elevation change is estimated through the error propagation law:~~

$$322 \delta_{dH} = \text{sqr}t(\delta_{\text{elev_diff}}^2 + n \times \delta_{\text{pene}}^2) \quad (2)$$

323 ~~Where elev_diff means the elevation difference, and pene means the penetration depth difference between C-band and X-~~
324 ~~band SRTM. The coefficient n is the factor between the C- and X-band penetration depth, which is 1 for the results of~~
325 ~~COP30 DEM – NASA DEM and 2 for the results of KH-9/HMA DEM – NASA DEM.~~

327 5.1 Identified surging glaciers

328 A total of 1226 surge-related glaciers across the HMA were identified based on the elevation changes and morphological
 329 changes. The identified surge-related glaciers consisted of 890 ‘verified’ surging ones, 208 ‘probable’ ones, and 128 ‘possible’
 330 ones. A total of 175 surging tributaries were identified in 86 glacier complexes. When merging the identification results of the
 331 two periods, we found that a considerable proportion of identified surging glaciers were simultaneously recognized in both
 332 periods. This makes our inventory more reliable since a surging glacier could exhibit different kinds of changes in different
 333 periods. For example, 26 probable and 51 possible surging glaciers identified during 2000-2020 turned out to be “verified”
 334 surging glaciers during 1970s-2000. Meanwhile, 60 “probable” and 21 “possible” surging glaciers identified during 1970s-
 335 2000 turned out to be ‘verified’ surging glaciers during 2000-2020. ~~Thanks~~Due to the almost complete coverage of elevation
 336 change observations, we were able to classify almost all glaciers in HMA. Table 42 shows the number of surging glaciers
 337 identified from two periods of elevation changes and morphological changes. Due to the incomplete coverage of KH-9 DEMs,
 338 103 identified surging glaciers have no observations during the period 1970s-2000. The data voids in KH-9 DEMs may be one
 339 of the reasons why fewer surging glaciers were identified in this period. In the following text, the “probable” and “possible”
 340 classes were deemed as surge-like glaciers, and only the “verified” surging glaciers were used for analysis and comparison
 341 throughout the rest of this study.

342 5.2 Distribution of surging glaciers

343 Surging glaciers were identified in 21 subregions of HMA (except for the Dzhungarsky Alatau); however, the spatial density
 344 of identified surging glaciers ~~is far from even (Fig. varies between different subregions (Figure 3))~~. Glacier surges are common
 345 in the northwest ern regions, sporadic in the inner regions, and scarce in the peripheral regions. Figure 4 and Table 2 show the
 346 ratios of surging glacier number and area in each subregion. Considering the area of the smallest identified surging glacier is
 347 0.42 km², we only ~~took the~~counted glaciers larger than 0.40 km² in the glacier number ~~related~~-ratio. When conducting statistical
 348 analysis, the surge-like glaciers were excluded from the dataset, ~~and~~ Besides, a surging tributary was regarded as an individual
 349 glacier. The number (890) and area (16556.42 km²) of identified surging glaciers accounted for ~2.49% and ~16.59% of the
 350 total glacier number and glacier area in HMA, respectively.

351 Among the 22 subregions, the Karakoram is the largest cluster of surging glaciers. In total 354 surging and 128 surge-like
 352 glaciers were identified in the Karakoram. The number and area of verified surging glaciers in the Karakoram accounted for
 353 39.80% and 47.90% of the total identified surging glaciers within HMA. We found that more than half of the tributary surges
 354 (101) occurred in the Karakoram, where large glaciers are much more developed than in other regions. In the Karakoram,
 355 although surging glaciers ~~have account for only~~ accounted for 8.59% of the total glacier number, their area occupied 39.48%
 356 of the total glacierized area. The Pamirs, composed of the Eastern Pamir, Western Pamir, and Pamir Alay, hosts 249 surging
 357 glaciers and 128 surge-like glaciers. About 27.74% of the glacier area in the Eastern and Western Pamir belongs to surging
 358 glaciers. We also found 28 surging tributaries in 15 glacier complexes in the Pamirs. Surging glaciers are also common in the
 359 Western Kunlun. In total 82 surging and 47 surge-like glaciers were identified in the West Kunlun, ~~and the area of surging~~
 360 ~~glaciers accounted for~~ representing 30.48% of the total glacier area. The Central Tien Shan has the fourth-largest surging glacier
 361 area. In total 59 surging glaciers were identified in the Central Tien Shan, ~~which covered~~ covering 12.93% of the total glacier
 362 area. The Karakoram, Pamirs, West Kunlun, and Central Tien Shan host ~83% of the surging glaciers across HMA. Figure 5
 363 shows the distribution of identified surging and surge-like glaciers in these four regions.

364 Within interior HMA subregions (including the Tibetan Interior Mountains, Eastern Kunlun Shan, and Tanggula Shan), ~~the~~
 365 ~~number of~~ identified surging glaciers represents less than 2% of the total number but ~~the area accounted for~~ nearly 15% of the
 366 total glacier area. ~~Surging glaciers~~ Glacier surges in these regions ~~are generally gathered~~ occurred in a few watersheds. Similar

367 localized surging glacier clusters were also found in the Nyainqentanglha, Northern, and Western Tien Shan, and Central
368 Himalaya, but the corresponding area ratios are much lower. In these regions, our inventory covered dozens of surging glaciers,
369 which were rarely reported before. Figure 6 shows some samples of identified surging glaciers in these regions.

370 5.3 Geometric characteristics of surging glaciers

371 In this part, only the surging glaciers and non-surging glaciers are taken for analysis. The surge-like glaciers are not included.
372 All glacier samples in the surging and non-surging classes are larger than 0.40 km².

373 We divided all glaciers into 9 classes according to their area, and calculated the ratios of surging glacier number and area in
374 each class. As shown in Figure 7 and Table 34, surging glaciers were found in all classes. Both the ratios of surging glacier
375 area and number became increasingly high as the glacier size increased, except for the last class. Surging glaciers with an area
376 of 1–50 km² occupy 82% of all surging glaciers. For the three classes in which glaciers are larger than 50 km², the ratios of
377 surging glaciers area and number were about 52% and 54%, respectively. In particular, 2 of 6 very large glaciers (the Siachen
378 glacier and the Hispar glacier) surged during our observation periods.

379 When comparing the geometric characteristics of the surging glaciers and non-surging glaciers, we selected samples in the
380 following way: for each surging glacier, we selected 10 non-surging glacier samples that have the closest area but from an
381 arbitrary region; and then we randomly sampled 3 out of the 10 selected non-surging glaciers. This is to minimize the
382 discrepancy resulting from the sample differences. There are two reasons for doing so. First, the gap between the sample
383 numbers is huge (~35000 non-surging vs. 890 surging). Second, a high proportion of non-surging glaciers are very small
384 glaciers. The final selected 890×3 non-surging glaciers formed the reference group.

~~385 We first analyzed the distribution of surging glacier number and area in eight orientations. As shown in Fig. 8, both the number
386 and area of glaciers facing the north are the largest, and then followed by those facing the northwest and northeast. The
387 distribution of the glacier orientation in the reference group was different from that of the non-surging glaciers, which
388 confirmed the statistical analysis would be affected by sample differences. The number of surging glaciers facing the north
389 accounted for ~30.1% of the total surging glacier number, and their area accounted for ~27.8% of all surging glacier area. The
390 number and area ratios of surging glaciers facing the north are obviously higher than that of the non-surging glaciers facing
391 north, while the number and area ratios of surging glaciers facing northwest are obviously lower than that of the non-surging
392 glaciers facing northwest. Meanwhile, the area ratio of surging glaciers facing northeast is considerably higher than the number
393 ratio, but for surging glaciers facing northwest and southwest, the situation is opposite.~~

394 Figure 98 illustrates the comparisons between the basic geometric properties of surging and non-surging glaciers. The sampling
395 strategy mentioned above was also utilized here. If we directly compare the surging glaciers with all non-surging glaciers, we
396 will find that surging glaciers generally have a larger area, wider elevation range (i.e., the highest glacier surface elevation
397 minus the lowest), and longer flow line (Fig 9a Figures 8a-c). Taking the median values as the candidates, the quantitative
398 comparisons are 7.3 km² (surging) vs. 0.87 km² (non-surging) for glacier area, 1534 m vs. 642 m for elevation range, and 6695
399 m vs. 1854 m for maximum glacier length, respectively. In terms of mean surface slope and median elevation, the values of
400 the surging glaciers are less spread out than the non-surging glaciers. However, the median values of the two kinds of glaciers
401 are very close (see Figures 9d8d and 9e8e). If we took the non-surging glaciers in the reference group for comparison, the
402 discrepancies between the two kinds of groups on these geometric properties became much more different. As shown in Figure
403 9a, the similar boxplots of the reference group and surging glacier samples proved that our sampling strategy has successfully
404 re-organized/corrected the bias in area between surging and non-surging glacier samples for comparisons. The gaps
405 between the surging and non-surging glaciers (reference group) in the glacier area (7.3 km² vs. 7.0 km²), elevation range (1534
406 m vs. 1180 m), and glacier length (6695 m vs. 5560 m), are much smaller. More importantly, the mean slope of the glaciers in
407 the reference group becomes smaller than that of the surging glaciers.

408 The correlation between different glacier geometric properties was analyzed through the bivariate scatterplots (see Figure 109).
409 Among the glacier area, glacier length, and glacier surface elevation range, any two of them have an apparent positive
410 correlation. The glacier mean slope has a moderate correlation with glacier area, length, and elevation range as they are auto-
411 correlated. By contrast, glacier median elevation has little correlation with these parameters. The correlation of any two
412 geometric properties makes little difference between surging and non-surging glaciers. All variables mentioned above are
413 embedded in the attribute table of the published inventory. Detailed descriptions of these variables can be found in Table 5.

414 6 Discussion

415 6.1 Uncertainty analysis

416 ~~The reliability of surging glacier identification is directly related to the accuracy of glacier surface elevation change. Assuming~~
417 ~~the uncertainties in surface elevation change are similar over glacierized areas and stable areas, we evaluated the glacier~~
418 ~~elevation change uncertainties based on elevation change observations in stable areas, whose true values are zeros. Meanwhile,~~
419 ~~the uncertainties in the radar penetration calculation were also considered through the error propagation law. The normalized~~
420 ~~median absolute deviation (NMAD) is less sensitive to outliers and can be deemed as a better proxy of uncertainty in dH than~~
421 ~~the standard deviation. Hence, the NMAD was used to denote the uncertainty of individual glacier surface elevation change~~
422 ~~tile. Figure 11 shows the NMAD of elevation change observations in stable areas within each DEM differencing tiles, which~~
423 ~~were used for the co-registration and biases removal during the glacier elevation change estimation. Due to large distortions~~
424 ~~in the KH-9 images, the NASADEM—KH-9 DEM results had the highest uncertainties. Benefiting from the advantages of~~
425 ~~bistatic SAR image pairs, the COP30 DEM has high quality, and the COP30 DEM related results had the lowest uncertainties.~~
426 ~~The HMA DEM related results had moderate uncertainties. The average NMAD of all DEM differencing tiles was smaller~~
427 ~~than 5 m. Significant elevation errors usually occurred in highly rugged regions such as crests and horns. The terrain of glacier~~
428 ~~surface is relatively gentle, and therefore the uncertainties of glacier surface elevation changes should be lower than the~~
429 ~~estimated values over the area where surges occur. The head of glaciers usually includes very steep faces and has a lot of~~
430 ~~uncertainties, but it does not matter too much for this study. In general, the uncertainties of our elevation change results are~~
431 ~~well-controlled. Figure 10 shows the uncertainties in four kinds of elevation difference observations and three kinds of glacier~~
432 ~~elevation change observations. The four kinds of elevation difference observations include three kinds of DEM difference~~
433 ~~observations and one kind of radar penetration depth difference observation. The uncertainties in glacier elevation change~~
434 ~~originated from the DEM difference and from the radar penetration depth difference. For each kind of elevation difference~~
435 ~~observation, the average uncertainty (NMAD) is generally smaller than 4.50 m, and the uncertainty of the penetration depth~~
436 ~~difference is the smallest. Due to the large distortion in the KH-9 images, the NASA DEM – KH-9 DEM results had the highest~~
437 ~~uncertainties. In general, the uncertainties of our elevation change results are acceptable. Compared with the typical surface~~
438 ~~elevation change resulting from a glacier surge (tens to hundreds of meters), the uncertainties are very small. For example, a~~
439 ~~large uncertainty in the KH-9 DEM related elevation change observation (say 8.00 m) is only about half of the threshold we~~
440 ~~used for identifying a ‘possible’ surging glacier.~~

441 ~~In order to illustrate the impact of topography on the uncertainty, we calculated the NMAD of COP30 DEM – NASA DEM~~
442 ~~difference over stable regions within different slope ranges (0-55°). As shown in Figure 11, the uncertainties in elevation~~
443 ~~difference observations increase as the terrain becomes steeper. Uncertainties over very steep regions (slope > 40°) can be two~~
444 ~~times larger than over flat terrain (slope < 10°). Therefore, dH observations over crests, horns, and heads of glaciers, generally~~
445 ~~have relatively large errors. In such regions, stereo optical images suffer from serious distortion, and sometimes have very low~~
446 ~~brightness contrast due to snow cover; in the meantime, SAR images are affected by shadows and layover (Pieczonka and~~
447 ~~Bolch, 2015) magnitudes of uncertainties are very small. However, the terrain of main glacier bodies where surges usually~~
448 ~~occur is gentler, and therefore the uncertainties of glacier surface elevation changes should be much lower than the thresholds~~

449 ~~that we used for identifying surges. Besides, the relatively large errors in dH maps are discontinuous in space, while the~~
450 ~~elevation changes used for identifying surges are spatially continuous. Hence, the uncertainty of glacier elevation change has~~
451 ~~no substantial impact on the identification of glacier surges.~~

452 Similar to previous studies (Sevestre and Benn, 2015; Goerlich et al., 2020), the surging glacier identification in this study
453 was completed through a manual qualitative interpretation. It ~~s~~ is difficult to provide a quantitative index to represent
454 the uncertainty of surge identification. However, ~~the four~~ we have assigned a three-class indicator ~~of to represent the~~
455 surge likelihood, which could aid that to a degree.

456 6.2 Characteristics of surging glaciers

457 The ~~direct~~ comparisons between geometric characteristics of surging and non-surging glaciers ~~manifest~~ show that surge activity
458 is more likely to occur in the glacier with a larger area, wider elevation range, and longer length (~~Fig. 9~~ Figures 7 and 8),
459 which is consistent with previous studies ~~also reported this phenomenon~~ (Barrand and Murray, 2006; Jiskoot, 2011; Sevestre
460 and Benn, 2015; Mukherjee et al., 2017; Guillet et al., 2022). ~~Larger area, wider elevation range, and longer length mean a~~
461 ~~larger glacier scale and more mass storage. Surge is a self-balancing process of a glacier to regulate its internal instability of~~
462 ~~thermal or hydrologic conditions which needs enough mass storage. In this case, about 97% of the surging glacier has an area~~
463 ~~larger than 1 km². For glaciers larger than 10 km², surge becomes a quite common behavior (with a number ratio higher than~~
464 ~~20%), rather than an accidental behavior (see Fig. 7).~~

465 ~~In terms of mean surface slope, we could not observe a statistically significant difference in the median value of the surging~~
466 ~~and non-surging glaciers, although the surging glaciers have a more concentrated value range (Fig. 9d and Figure 10, 3rd row,~~
467 ~~1st column). After minimizing this kind of bias, we observed an obviously higher mean slope of surging glaciers in the~~
468 ~~comparison with the reference group. Several studies have demonstrated that the surging glacier tends~~ Several studies have
469 demonstrated that surging glaciers tend to have a shallower slope (Jiskoot et al., 2000; Guillet et al., 2022). However, ~~here~~ we
470 reasonably argue that this rule was concluded from an unbalanced comparison, as non-surging glaciers have a higher proportion
471 of small glaciers than surging glaciers. Meanwhile, the inverse relationship between the glacier slope and length (Clarke, 1991;
472 Sevestre and Benn, 2015) may not apply to very small glaciers (i.e. smaller than 1 km²). As shown in ~~Fig. 9d and Fig. 10,~~
473 among the non-surging glaciers, the small ones occupy a high proportion and their mean ~~slope presents~~ slopes have strong
474 variability. ~~Regarding this~~ Thus, we can conclude that steeper glaciers are more likely to surge when the comparison is restricted
475 to similar areas. As for the glacier median elevation, since it is almost ~~irrelevant~~ uncorrelated to the glacier area, glacier length,
476 glacier elevation range, and glacier mean slope (see ~~Fig. 10~~ Figure 9), it can be deemed as an irregular glacier index. However,
477 among glaciers that have similar areas, steeper glaciers generally have a lower median elevation. That's why the median
478 elevation of surging glaciers is slightly smaller than that of non-surging glaciers (~~Fig. 9e~~ Figure 8e).

479 These comparisons could now lead to a conclusion as follows: the surging glaciers are generally longer, and have a larger
480 elevation range than non-surging glaciers, since they have more mass storage. However, when glaciers are similar in area, a
481 steeper surface slope is more likely to lead to surge.

482 ~~Besides, our results highlight that the ratio distribution of surging glaciers in eight aspects is slightly different from that of~~
483 ~~non-surging glaciers (see Fig. 8). Overall, the ratio of surging glaciers is relatively higher than the non-surging glaciers in the~~
484 ~~north and northeast directions, but lower in the northwest direction. It is generally known that glaciers facing north are more~~
485 ~~developed in HMA. Due to the orientation of the mountains, most of the large glaciers flow toward north and northeast. Besides,~~
486 ~~the area to number ratio of surging glaciers is much larger than non-surging glaciers in the northeast orientation, but smaller~~
487 ~~in the northwest orientation. This is true for the Karakoram, Pamirs, and West Kunlun Shan, the three largest clusters of surging~~
488 ~~glaciers, indicating that large northeast-facing glaciers have a higher chance to be surging glaciers. Accordingly, the surging~~
489 ~~glaciers facing north and northeast have a higher area ratio than that facing the northwest.~~

490 The spatial distribution of surging glaciers in HMA presents a strong heterogeneity. About 83% of identified surging glaciers
491 ~~we~~ are located in the northwest ~~ern~~ region including the Central Tien Shan, Pamirs, Karakoram, and West Kunlun, and ~~their~~
492 ~~area occupied~~ they occupy about 87% of the total identified surging glacier area (see Fig-~~ure~~ 4 and Table 23). As discussed
493 above, larger glaciers are more likely to surge. The northwest regions generally hold ~~more large~~ larger glaciers- and therefore
494 hold more surging glaciers. In other subregions, large glaciers are usually concentrated in some great ice fields, such as the
495 Geladandong, Puruogangri, and Xinqingfeng. ~~Accordingly,~~ Surging glaciers in these subregions are usually clustered in
496 ~~several~~ a few watersheds.

497 ~~Several studies have pointed out that glacier surge activities have little impact on the glacier mass balance . However, glacier~~
498 ~~mass balance may also affect the occurrence of glacier surges. Copland et al. concluded that the increase of glacier surges in~~
499 ~~the Karakoram could be related to the positive mass budget. The accumulated ice mass would accelerate a glacier to surge ,~~
500 ~~and the significant mass loss could prevent or postpone the surge in return . On a regional large scale, the relationship between~~
501 ~~mass balance and surge occurrence needs to be further analyzed. Our glacier elevation change maps of the period 2000-2010s~~
502 ~~are similar to that derived by Brun et al. and Shean et al. . We found that, at the regional scale, the occurrence of surging~~
503 ~~glaciers is correlated with the regional glacier mass balance. The three subregions holding the largest clusters of surging~~
504 ~~glaciers, i.e., the Pamirs, Karakoram, and West Kunlun, are characterized by slightly negative or positive elevation changes,~~
505 ~~which is known as one part of the ‘Pamir Karakoram West Kunlun’ anomaly . Likewise, the subregions Central Tien Shan,~~
506 ~~Tibetan Interior Mountains, and East Kunlun Shan, which hold the moderate clusters of surging glaciers, have glacier mass~~
507 ~~loss rates much lower than the average rates of HMA. By contrast, subregions with severe glacier mass loss hold the lowest~~
508 ~~surging glacier ratio, such as the Dzhungarsky Alatau, Hengduan Shan, and Eastern Himalaya.~~

509 6.3 Comparison with previous surging glacier inventories

510 Guillet et al. (2022) presented a comprehensive surging glacier inventory of HMA for the period 2000-2018 from a multi-
511 factor remote sensing approach. Prior to the comparison, we generated an inventory based on the RGI6.0, as Guillet et al.
512 (2022) did. Guillet et al. (2022) identified 666 surging glaciers, ~~and the area of surging glaciers occupies~~ covering 19.5% of
513 the total glacier area. We identified 890 surging glaciers (809 if represented by RGI6.0 polygons), ~~and their area only~~
514 ~~occupies~~ covering 16.59% of the total glacier area. We attributed the lower area ratio of surging glaciers to two reasons. First,
515 in our inventory, the surging tributaries were separated from the non-surging trunks. Second, many outcrop rocks and shaded
516 areas are excluded from the GAMDAM2 glacier areas (Sakai, 2019), which would lower our surging area ratio, but make the
517 result more accurate. If we assign our identified surging glaciers to the RGI6.0 polygons without tributary separation, the
518 surging area ratio would be larger (20.25%).

519 Within our inventory, 556 surging and 62 surge-like glaciers were also identified by Guillet et al. (2022), and the discrepancy
520 of identifications mostly occurred on small glaciers. If only the period 2000-2020 was considered, 657 surging glaciers were
521 identified by us, which is very close to that of Guillet et al. (665~~6~~). For the period 1970s-2000, we found 151 surging and 101
522 surge-like glaciers that were not identified by Guillet et al. (2022). Overall, we have newly identified 253 surging and 248
523 surge-like glaciers. We owed the new findings to the longer observation period and multiple elevation change observations.
524 However, 47 surging glaciers presented by Guillet et al. were missed in this study, and 62 surge-like glaciers in our new
525 inventory were identified as surging glaciers by Guillet et al. (2022). We ~~carefully~~ checked the glaciers not included in our
526 inventory but included in the inventory of Guillet et al. (2022) ~~s inventory,~~ as well as those included in our inventory but not
527 included in Guillet et al.'s inventory, and this step helped us to find 21 more surging glaciers. We attribute this to the ~~deficiency~~
528 ~~of using a single~~ missing criterion of flow velocities, which could ~~be aided by combining other features~~ capture some small
529 surges without obvious elevation change or morphological change. Besides, the DEMs used in this study were suffering from
530 data voids and incomplete spatial coverage, especially for the KH-9 DEM, which could result in a relatively conservative
531 identification.

532 Multiple studies have identified surging glaciers in the Karakoram based on different data sources. For example, Bhambri et
533 al. (2017) identified 221 surging and surge-like glaciers (counting tributaries of a glacier system as individual glaciers) based
534 on glacier morphological changes detected from space-borne optical images acquired from 1972 to 2016, in-situ observations,
535 and archive photos dating back to the 1840s. However, the boundary used by Bhambri et al. (2017) to define the extent of
536 Karakoram is much smaller than that used in our inventory. A much smaller group of surging glaciers (88) was identified by
537 Copland et al. (2011) based on a similar method and the data acquired between 1960 and 2013. Rankl et al. (2014) identified
538 101 surging glaciers in the Karakoram by detecting changes in glacier surface velocity and terminus position between 1976
539 and 2012. The results of Guillet et al. (2022) should be more reliable than previous ones because more criteria were used for
540 identifying surging glaciers. Compared with previous inventories, our inventory includes more surging glaciers in the
541 Karakoram (354). Among the 223 surging glaciers in the Karakoram identified by Guillet et al. (2022), 203 were identified as
542 surging glaciers, and 12 were identified as surge-like glaciers in this study, which means only 8 surging glaciers presented by
543 Guillet et al. (2022) were not included in our inventory. The high coincidence between the two inventories indicates our surging
544 glacier identification result is reliable. In total, we have newly identified 101 surging and 101 surge-like glaciers in this region.
545 Based on the method of glacier terminus change monitoring in Google Earth Engine, Vale et al. (2021) identified
546 ~~obvious changes in the~~ terminus ~~change~~ of 137 surging glaciers. ~~We found that~~ In total, 127 verified surging and 6 surge-like
547 glaciers in our inventory were included in their inventory, i.e., only four glaciers were missed in this study. ~~The possible reason~~
548 ~~for this gap is that the technique used by Vale et al. cannot identify the internal glacier surges that did not result in a terminus~~
549 ~~advance. Also, the inadequate quality and spatial resolution of satellite images could limit the performance of detecting changes~~
550 ~~in glacier terminus position. We found these four missing surging glaciers had slight terminus advancing (<200 m) during long~~
551 ~~surging periods (>10 years). The very slow and slight terminus advance is difficult to identify through visual interpretation.~~
552 In the Pamirs, Sevestre and Beenn (2015) identified 820 surge-type glaciers based on publications and reports, but Goerlich et
553 al. (2020) reported only 186 surging glaciers based on observations of glacier flow velocity, elevation change, etc. We found
554 that if Goerlich et al. (2020) applied the GAMDAM2 glacier polygons used in this study, the number of identified surging
555 glaciers would be 182. Among the 182 surging glaciers identified by Goerlich et al. (2020), 153 were identified as surging
556 glaciers and 15 were identified as surge-like glaciers in our study. Although 14 surging glaciers are missed in this study, our
557 inventory ~~has contained other~~ contains another 94 surging and 44 surge-like glaciers. The main cause for the discrepancy is
558 that the glacier elevation change observations s before 2000 ~~conducted~~ used by Goerlich et al. (2020) only covered ~~ed~~ a small part
559 of the Western Pamir. In this region, our inventory shared 193 surging glaciers with Guillet et al.'s inventory, and 185 of them
560 were identified during the period 2000-2020, which also manifests a high coincidence of the two results.
561 In the West Kunlun, Yasuda and Furuya (2015) reported 9 surging glaciers in the main range only, based on changes in glacier
562 flow velocity and terminus position of 31 glaciers, and another 9 surging glaciers were found in the northwest part of the West
563 Kunlun Shan by Chudley et al. (2019). A larger number (60) were found by Guillet et al. (2022). However, our inventory
564 ~~has includes~~ even included more surging (82) and surge-like (47) glaciers in the West Kunlun Shan. ~~During~~ For the period
565 2000-2020, we ~~have~~ identified 61 surging glaciers, which is very close to the number presented by Guillet et al. (2022). In
566 Central Tien Shan, Mukherjee et al. (2017) identified 39 surge-type (including 9 surging and 13 very probable surging) glaciers
567 through the analysis of changes in surface elevation and morphology from 1964 to 2014, whereas 79 (59 surging and 20 surge-
568 like) were identified in our studies. The insufficient coverage of elevation change observation (only covering the west part of
569 the Central Tien Shan) may be the main reason for the discrepancy in identification results. Guillet et al. (2022) identified 54
570 surging glaciers during 2000-2018, ~~in~~ from which 36 were confirmed in our inventory.

571 7 Conclusions

572 This study presents a new inventory of surging glaciers across the entire HMA range, ~~which was accomplished based on the~~
573 ~~For the surge identification, we relied on~~ glacier surface elevation changes derived from multiple elevation sources, ~~by using~~
574 ~~the and complementarily on optical satellite images for assessing~~ morphological changes ~~from optical images as complements~~.
575 In total, 890 surging and 336 probably or possibly surging glaciers were identified in the new inventory. Through the analysis
576 of geometric parameters, we found that surging glaciers generally have a greater area, length, and elevation range than non-
577 surging glaciers. However, the differences are smaller when taking the glacier size distribution into account. When considering
578 glaciers of similar areas, the steeper ones are more likely to surge. ~~Furthermore, by combining the region-wide glacier mass~~
579 ~~balance measurements, we found a similar distribution between the positive mass balance and the number of surging glaciers.~~
580 Benefiting from the long period and wide coverage of surface elevation change observations, our study newly identified 253
581 surging and 248 surge-like glaciers in HMA ~~than compared to~~ the previous inventory (Guillet et al., 2022). However, our
582 inventory does not provide the surge duration period and the maximum flow velocity, ~~which are useful~~ to describe the dynamic
583 process of each glacier surge activity. Improvements should be made by combining multi-criteria identification methods.
584 Considering the fact that glacier surges are more widespread than we thought, the inventory presented in this study still needs
585 further ~~replenishment~~ improvement.

586 8 Data and code availability

587 The presented inventory and ~~corresponding the~~ multi-temporal elevation change results ~~of identified used to identify~~ surging
588 glaciers are freely available at: <https://doi.org/10.5281/zenodo.7961207-7950838> (Guo et al., 2022). The inventory ~~is~~
589 ~~distributed in the format of GeoPackage (.gpkg) and ESRI shapefile (.shp), which is represented by contains glacier~~ outlines
590 and manually defined center points of surging glaciers with geometric attributes ~~and is distributed in GeoPackage (.gpkg) and~~
591 ~~ESRI shapefile (.shp) formats~~. The glacier polygons ~~of the inventory~~ are compiled from the GAMDAM2 glacier inventory. In
592 total, eight fields are integrated into the attributes table to describe the surging information of the corresponding glacier as
593 mentioned in section 4.3. The description of each field in the attribute table is listed in Table 4. The DEM ~~differencing~~
594 ~~results of the differences (COP30 DEM – NASA_DEM, HMA DEM – NASA_DEM, and NASA_DEM – KH-9 DEM)~~ are
595 compressed into individual zip files, respectively. The elevation change results of surging glaciers were divided into multi-
596 temporal $1^\circ \times 1^\circ$ tiled GeoTiff grids. The metadata file is stored in a text file (README.txt), which contains the datasets
597 description and details of the attribute information of the inventory.
598 The code used for elevation change estimation ~~can be is~~ available at: https://github.com/TristanBlus/dem_coreg. This code was
599 developed based on the *demcoreg* package (Shean et al., 2019).

600 Author contribution

601 J.L. and L.G. conceived this study and wrote the paper. L.G. developed the processing flow, compiled the inventory, and drew
602 the figures with support from J.L. A.D. generated the KH-9 DEM. A.D., Z.L., and X.L. helped with the results analysis and
603 discussions, as well as manuscript editing. Z.L., J.L., and J.Z. provided funding acquisition. All authors have contributed and
604 agreed to the published version of the manuscript.

605 Competing interest

606 The authors declare that they have no conflict of interest.

607 Acknowledgments

608 The authors express their gratitude to all institutions that provide us with the ~~open sourcee dataset~~ open source datasets used in
609 this study: the NASA DEM from LP DAAC (https://e4ftl01.cr.usgs.gov/MEASURES/NASADEM_HGT.001/), the
610 Copernicus DEM from the European Space Agency (ESA) (<https://spacedata.copernicus.eu/web/cscda/cop-dem-faq>), the
611 HMA DEM processed by David Shean from National Snow and Ice Data Center (NSIDC)
612 (https://nsidc.org/data/HMA_DEM8m_MOS/versions/1), and the Randolph Glacier Inventory Version 6.0
613 (<http://www.glims.org/RGI/randolph.html>). The authors also appreciate the valuable comments from Frank Paul and Grégoire
614 Guillet-Gregoire.

615 Financial support

616 This work was supported by the Strategic Priority Research Program of Chinese Academy of Sciences (XDA20100101), the
617 National Natural Science Fund for Distinguished Young Scholars (41925016), the Hunan Key Laboratory of Remote Sensing
618 of Ecological Environment in Dongting Lake Area (No. 2021-010), the National Natural Science Foundation of China
619 (41904006), the Fundamental Research Funds for the Central Universities of Central South University (2021zzts0265).

620 References

- 621 Abdel Jaber, W., Rott, H., Floricioiu, D., Wuite, J., and Miranda, N.: Heterogeneous spatial and temporal pattern of surface
622 elevation change and mass balance of the Patagonian ice fields between 2000 and 2016, *The Cryosphere*, 13, 2511–2535,
623 doi:10.5194/tc-13-2511-2019, 2019.
- 624 AIRBUS: Copernicus Digital Elevation Model Validation Report, AIRBUS Defence and Space GmbH, 2020.
- 625 Barrand, N. E. and Murray, T.: Multivariate Controls on the Incidence of Glacier Surging in the Karakoram Himalaya, *Arct.*
626 *Antarct. Alp. Res.*, 38, 489–498, doi:10.1657/1523-0430(2006)38[489:MCOTIO]2.0.CO;2, 2006.
- 627 Beaud, F., Aati, S., Delaney, I., Adhikari, S., and Avouac, J.-P.: Generalized sliding law applied to the surge dynamics of
628 Shisper Glacier and constrained by timeseries correlation of optical satellite images, *Glaciers/Remote Sensing*, doi:10.5194/tc-
629 2021-96, 2021.
- 630 Benn, D. I., Fowler, A. C., Hewitt, I., and Sevestre, H.: A general theory of glacier surges, *J. Glaciol.*, 65, 701–716,
631 doi:10.1017/jog.2019.62, 2019.
- 632 Bhambri, R., Hewitt, K., Kawishwar, P., and Pratap, B.: Surge-type and surge-modified glaciers in the Karakoram, *Sci. Rep.*,
633 7, doi:10.1038/s41598-017-15473-8, 2017.
- 634 Bhambri, R., Hewitt, K., Haritashya, U. K., Chand, P., Kumar, A., Verma, A., Tiwari, S. K., and Rai, S. K.: Characteristics of
635 surge-type tributary glaciers, Karakoram, *Geomorphology*, 403, 108161, doi:10.1016/j.geomorph.2022.108161, 2022.
- 636 Bolch, T., Kulkarni, A., Kaab, A., Huggel, C., Paul, F., Cogley, J. G., Frey, H., Kargel, J. S., Fujita, K., Scheel, M., Bajracharya,
637 S., and Stoffel, M.: The State and Fate of Himalayan Glaciers, *Science*, 336, 310–314, doi:10.1126/science.1215828, 2012.
- 638 Bolch, T., Pieczonka, T., Mukherjee, K., and Shea, J.: Brief communication: Glaciers in the Hunza catchment (Karakoram)
639 have been nearly in balance since the 1970s, *The Cryosphere*, 11, 531–539, doi:10.5194/tc-11-531-2017, 2017.
- 640 Bolch, T., Shea, J. M., Liu, S., Azam, F. M., Gao, Y., Gruber, S., Immerzeel, W. W., Kulkarni, A., Li, H., Tahir, A. A., Zhang,
641 G., and Zhang, Y.: Status and Change of the Cryosphere in the Extended Hindu Kush Himalaya Region, in: *The Hindu Kush*
642 *Himalaya Assessment*, edited by: Wester, P., Mishra, A., Mukherji, A., and Shrestha, A. B., Springer International Publishing,
643 Cham, 209–255, doi:10.1007/978-3-319-92288-1_7, 2019.
- 644 Brun, F., Berthier, E., Wagnon, P., Käab, A., and Treichler, D.: A spatially resolved estimate of High Mountain Asia glacier
645 mass balances from 2000 to 2016, *Nat. Geosci.*, 10, 668–673, doi:10.1038/ngeo2999, 2017.

646 Chudley, T. R. and Willis, I. C.: Glacier surges in the north-west West Kunlun Shan inferred from 1972 to 2017 Landsat
647 imagery, *J. Glaciol.*, 65, 1–12, doi:10.1017/jog.2018.94, 2019.

648 Clarke, G. K. C.: Length, width and slope influences on glacier surging, *J. Glaciol.*, 37, 236–246,
649 doi:10.3189/S0022143000007255, 1991.

650 Clarke, G. K. C., Schmok, J. P., Ommanney, C. S. L., and Collins, S. G.: Characteristics of surge-type glaciers, *J. Geophys.*
651 *Res. Solid Earth*, 91, 7165–7180, doi:10.1029/JB091iB07p07165, 1986.

652 Cogley, J. G., Arendt, A. A., Bauder, A., Braithwaite, R. J., Hock, R., J, B., R., Jansson, P., Kaser, G., Moller, M., Nicholson,
653 L., Rasmussen, L. A., and Zemp, M.: Glossary of glacier mass balance and related terms, IACS Contribution No.2, UNESCO,
654 Paris, 2011.

655 Copland, L., Sylvestre, T., Bishop, M. P., Shroder, J. F., Seong, Y. B., Owen, L. A., Bush, A., and Kamp, U.: Expanded and
656 Recently Increased Glacier Surging in the Karakoram, *Arct. Antarct. Alp. Res.*, 43, 503–516, 2011.

657 Crippen, R., Buckley, S., Agram, P., Belz, E., Gurrola, E., Hensley, S., Kobrick, M., Lavallo, M., Martin, J., Neumann, M.,
658 Nguyen, Q., Rosen, P., Shimada, J., Simard, M., and Tung, W.: NASADEM global elevation model: methods and progress,
659 *ISPRS - Int. Arch. Photogramm. Remote Sens. Spat. Inf. Sci.*, XLI-B4, 125–128, doi:10.5194/isprsarchives-XLI-B4-125-2016,
660 2016.

661 Dehecq, A., Gardner, A. S., Alexandrov, O., McMichael, S., Hugonnet, R., Shean, D., and Marty, M.: Automated Processing
662 of Declassified KH-9 Hexagon Satellite Images for Global Elevation Change Analysis Since the 1970s, *Front. Earth Sci.*, 8,
663 566802, doi:10.3389/feart.2020.566802, 2020.

664 Fan, Y., Ke, C.-Q., Zhou, X., Shen, X., Yu, X., and Lhakpa, D.: Glacier mass-balance estimates over High Mountain Asia
665 from 2000 to 2021 based on ICESat-2 and NASADEM, *J. Glaciol.*, 1–13, doi:10.1017/jog.2022.78, 2022.

666 Farinotti, D., Immerzeel, W. W., Kok, R., Quincey, D. J., and Dehecq, A.: Manifestations and mechanisms of the Karakoram
667 glacier Anomaly, *Nat. Geosci.*, 13, 8–16, doi:10.1038/s41561-019-0513-5, 2020.

668 Farnsworth, W. R., Ingólfsson, Ó., Retelle, M., and Schomacker, A.: Over 400 previously undocumented Svalbard surge-type
669 glaciers identified, *Geomorphology*, 264, 52–60, doi:10.1016/j.geomorph.2016.03.025, 2016.

670 Farr, T. G., Rosen, P. A., Caro, E., Crippen, R., Duren, R., Hensley, S., Kobrick, M., Paller, M., Rodriguez, E., Roth, L., Seal,
671 D., Shaffer, S., Shimada, J., Umland, J., Werner, M., Oskin, M., Burbank, D., and Alsdorf, D.: The Shuttle Radar Topography
672 Mission, *Rev. Geophys.*, 45, RG2004, doi:10.1029/2005RG000183, 2007.

673 Fowler, A. C.: A theory of glacier surges, *J. Geophys. Res.*, 92, 9111, doi:10.1029/JB092iB09p09111, 1987.

674 Fowler, A. C., Murray, T., and Ng, F. S. L.: Thermally controlled glacier surging, *J. Glaciol.*, 47, 527–538,
675 doi:10.3189/172756501781831792, 2001.

676 Gardelle, J., Berthier, E., Arnaud, Y., and Käab, A.: Region-wide glacier mass balances over the Pamir-Karakoram-Himalaya
677 during 1999–2011, *Cryosphere Discuss.*, 7, 975–1028, doi:10.5194/tcd-7-975-2013, 2013.

678 Goerlich, F., Bolch, T., and Paul, F.: More dynamic than expected: an updated survey of surging glaciers in the Pamir, *Earth*
679 *Syst. Sci. Data*, 12, 3161–3176, doi:10.5194/essd-12-3161-2020, 2020.

680 Guillet, G., King, O., Lv, M., Ghuffar, S., Benn, D., Quincey, D., and Bolch, T.: A regionally resolved inventory of High
681 Mountain Asia surge-type glaciers, derived from a multi-factor remote sensing approach, *The Cryosphere*, 16, 603–623,
682 doi:10.5194/tc-16-603-2022, 2022.

683 Guth, P. L. and Geoffroy, T. M.: LiDAR point cloud and ICESat-2 evaluation of 1 second global digital elevation models:
684 Copernicus wins, *Trans. GIS*, 25, 2245–2261, doi:10.1111/tgis.12825, 2021.

685 Hewitt, K.: The Karakoram Anomaly? Glacier Expansion and the ‘Elevation Effect,’ *Karakoram Himalaya, Mt. Res. Dev.*, 25,
686 332–340, doi:10.1659/0276-4741(2005)025[0332:TKAGEA]2.0.CO;2, 2005.

687 Hewitt, K.: Tributary glacier surges: an exceptional concentration at Panmah Glacier, Karakoram Himalaya, *J. Glaciol.*, 53,
688 181–188, doi:10.3189/172756507782202829, 2007.

689 Höhle, J. and Höhle, M.: Accuracy assessment of digital elevation models by means of robust statistical methods, *ISPRS J.*
690 *Photogramm. Remote Sens.*, 64, 398–406, doi:10.1016/j.isprsjprs.2009.02.003, 2009.

691 Holzer, N., Vijay, S., Yao, T., Xu, B., Buchroithner, M., and Bolch, T.: Four decades of glacier variations at Muztagh Ata
692 (eastern Pamir): a multi-sensor study including Hexagon KH-9 and Pléiades data, *The Cryosphere*, 9, 2071–2088,
693 doi:10.5194/tc-9-2071-2015, 2015.

694 Hugonnet, R., McNabb, R., Berthier, E., Menounos, B., Nuth, C., Girod, L., Farinotti, D., Huss, M., Dussailant, I., Brun, F.,
695 and Kääb, A.: Accelerated global glacier mass loss in the early twenty-first century, *Nature*, 592, 726–731,
696 doi:10.1038/s41586-021-03436-z, 2021.

697 Jacquemart, M. and Cicoira, A.: Hazardous Glacier Instabilities: Ice Avalanches, Sudden Large-Volume Detachments of Low-
698 Angle Mountain Glaciers, and Glacier Surges, in: *Treatise on Geomorphology*, Elsevier, 330–345, doi:10.1016/B978-0-12-
699 818234-5.00188-7, 2022.

700 Jiskoot, H.: Glacier Surging, in: *Encyclopedia of Snow, Ice and Glaciers*, edited by: Singh, V. P., Singh, P., and Haritashya,
701 U. K., Springer Netherlands, Dordrecht, 415–428, doi:10.1007/978-90-481-2642-2_559, 2011.

702 Jiskoot, H., Murray, T., and Boyle, P.: Controls on the distribution of surge-type glaciers in Svalbard, *J. Glaciol.*, 46, 412–422,
703 doi:10.3189/172756500781833115, 2000.

704 Kamb, B.: Glacier surge mechanism based on linked cavity configuration of the basal water conduit system, *J. Geophys. Res.*,
705 92, 9083, doi:10.1029/JB092iB09p09083, 1987.

706 Leclercq, P. W., Kääb, A., and Altena, B.: Brief communication: Detection of glacier surge activity using cloud computing of
707 Sentinel-1 radar data, *The Cryosphere*, 15, 4901–4907, doi:10.5194/tc-15-4901-2021, 2021.

708 Li, J., Li, Z., Zhu, J., Li, X., Xu, B., Wang, Q., Huang, C., and Hu, J.: Early 21st century glacier thickness changes in the
709 Central Tien Shan, *Remote Sens. Environ.*, 192, 12–29, doi:10.1016/j.rse.2017.02.003, 2017.

710 Lv, M., Guo, H., Lu, X., Liu, G., Yan, S., Ruan, Z., Ding, Y., and Quincey, D. J.: Characterizing the behaviour of surge- and
711 non-surge-type glaciers in the Kingata Mountains, eastern Pamir, from 1999 to 2016, *The Cryosphere*, 13, 219–236,
712 doi:10.5194/tc-13-219-2019, 2019.

713 Lv, M., Guo, H., Yan, J., Wu, K., Liu, G., Lu, X., Ruan, Z., and Yan, S.: Distinguishing Glaciers between Surging and
714 Advancing by Remote Sensing: A Case Study in the Eastern Karakoram, *Remote Sens.*, 12, 2297, doi:10.3390/rs12142297,
715 2020.

716 Maurer, J. M., Schaefer, J. M., Rupper, S., and Corley, A.: Acceleration of ice loss across the Himalayas over the past 40 years,
717 *Sci. Adv.*, 5, eaav7266, doi:10.1126/sciadv.aav7266, 2019.

718 Maussion, F., Scherer, D., Mölg, T., Collier, E., Curio, J., and Finkelnburg, R.: Precipitation Seasonality and Variability over
719 the Tibetan Plateau as Resolved by the High Asia Reanalysis, *J. Clim.*, 27, 1910–1927, doi:10.1175/JCLI-D-13-00282.1, 2014.

720 Maussion, F., Butenko, A., Champollion, N., Dusch, M., Eis, J., Fourteau, K., Gregor, P., Jarosch, A. H., Landmann, J.,
721 Oesterle, F., Recinos, B., Rothenpieler, T., Vlug, A., Wild, C. T., and Marzeion, B.: The Open Global Glacier Model (OGGM)
722 v1.1, *Geosci. Model Dev.*, 12, 909–931, doi:10.5194/gmd-12-909-2019, 2019.

723 Mukherjee, K., Bolch, T., Goerlich, F., Kutuzov, S., Osmonov, A., Pieczonka, T., and Shesterova, I.: Surge-Type Glaciers in
724 the Tien Shan (Central Asia), *Arct. Antarct. Alp. Res.*, 49, 147–171, doi:10.1657/AAAR0016-021, 2017.

725 Murray, T., Strozzi, T., Luckman, A., Jiskoot, H., and Christakos, P.: Is there a single surge mechanism? Contrasts in dynamics
726 between glacier surges in Svalbard and other regions: IS THERE A SINGLE SURGE MECHANISM?, *J. Geophys. Res. Solid*
727 *Earth*, 108, doi:10.1029/2002JB001906, 2003.

728 Nuimura, T., Sakai, A., Taniguchi, K., Nagai, H., Lamsal, D., Tsutaki, S., Kozawa, A., Hoshina, Y., Takenaka, S., Omiya, S.,
729 Tsunematsu, K., Tshering, P., and Fujita, K.: The GAMDAM glacier inventory: a quality-controlled inventory of Asian
730 glaciers, *The Cryosphere*, 9, 849–864, doi:10.5194/tc-9-849-2015, 2015.

731 Nuth, C. and Kääb, A.: Co-registration and bias corrections of satellite elevation data sets for quantifying glacier thickness
732 change, *The Cryosphere*, 5, 271–290, doi:10.5194/tc-5-271-2011, 2011.

733 Paul, F.: Revealing glacier flow and surge dynamics from animated satellite image sequences: examples from the Karakoram,
734 *The Cryosphere*, 9, 2201–2214, doi:10.5194/tc-9-2201-2015, 2015.

735 Pieczonka, T. and Bolch, T.: Region-wide glacier mass budgets and area changes for the Central Tien Shan between ~1975
736 and 1999 using Hexagon KH-9 imagery, *Glob. Planet. Change*, 128, 1–13, doi:10.1016/j.gloplacha.2014.11.014, 2015.

737 Purinton, B. and Bookhagen, B.: Beyond Vertical Point Accuracy: Assessing Inter-pixel Consistency in 30 m Global DEMs
738 for the Arid Central Andes, *Front. Earth Sci.*, 9, 758606, doi:10.3389/feart.2021.758606, 2021.

739 Quincey, D. J., Braun, M., Glasser, N. F., Bishop, M. P., Hewitt, K., and Luckman, A.: Karakoram glacier surge dynamics,
740 *Geophys. Res. Lett.*, 38, L18504, doi:10.1029/2011GL049004, 2011.

741 Rankl, M., Kienholz, C., and Braun, M.: Glacier changes in the Karakoram region mapped by multitemporal satellite imagery,
742 *The Cryosphere*, 8, 977–989, doi:10.5194/tc-8-977-2014, 2014.

743 Rott, H., Sturm, K., and Miller, H.: Active and passive microwave signatures of Antarctic firn by means of field measurements
744 and satellite data, *Ann. Glaciol.*, 17, 337–343, doi:10.3189/S026030500013070, 1993.

745 Round, V., Leinss, S., Huss, M., Haemmig, C., and Hajsek, I.: Surge dynamics and lake outbursts of Kyagar Glacier,
746 Karakoram, *The Cryosphere*, 11, 723–739, doi:10.5194/tc-11-723-2017, 2017.

747 Sakai, A.: Brief communication: Updated GAMDAM glacier inventory over high-mountain Asia, *The Cryosphere*, 13, 2043–
748 2049, doi:10.5194/tc-13-2043-2019, 2019.

749 Sevestre, H. and Benn, D. I.: Climatic and geometric controls on the global distribution of surge-type glaciers: implications
750 for a unifying model of surging, *J. Glaciol.*, 61, 646–662, doi:10.3189/2015JoG14J136, 2015.

751 Shean, D., Shashank Bhushan, Lilien, D., and Meyer, J.: dshean/demcoreg: Zenodo DOI release, ,
752 doi:10.5281/ZENODO.3243481, 2019.

753 Shean, D. E., Alexandrov, O., Moratto, Z. M., Smith, B. E., Joughin, I. R., Porter, C., and Morin, P.: An automated, open-
754 source pipeline for mass production of digital elevation models (DEMs) from very-high-resolution commercial stereo satellite
755 imagery, *ISPRS J. Photogramm. Remote Sens.*, 116, 101–117, doi:10.1016/j.isprsjprs.2016.03.012, 2016.

756 Shean, D. E., Bhushan, S., Montesano, P., Rounce, D. R., Arendt, A., and Osmanoglu, B.: A Systematic, Regional Assessment
757 of High Mountain Asia Glacier Mass Balance, *Front. Earth Sci.*, 7, 363, doi:10.3389/feart.2019.00363, 2020.

758 Surazakov, A. and Aizen, V.: Positional Accuracy Evaluation of Declassified Hexagon KH-9 Mapping Camera Imagery,
759 *Photogramm. Eng. Remote Sens.*, 76, 603–608, doi:10.14358/PERS.76.5.603, 2010.

760 Thøgersen, K., Gilbert, A., Schuler, T. V., and Malthe-Sørenssen, A.: Rate-and-state friction explains glacier surge propagation,
761 *Nat. Commun.*, 10, 2823, doi:10.1038/s41467-019-10506-4, 2019.

762 Vale, A. B., Arnold, N. S., Rees, W. G., and Lea, J. M.: Remote Detection of Surge-Related Glacier Terminus Change across
763 High Mountain Asia, *Remote Sens.*, 13, 1309, doi:10.3390/rs13071309, 2021.

764 Van Wyk de Vries, M., Wickert, A. D., MacGregor, K. R., Rada, C., and Willis, M. J.: Atypical landslide induces speedup,
765 advance, and long-term slowdown of a tidewater glacier, *Geology*, doi:10.1130/G49854.1, 2022.

766 Yamazaki, D., Ikeshima, D., Tawatari, R., Yamaguchi, T., O’Loughlin, F., Neal, J. C., Sampson, C. C., Kanae, S., and Bates,
767 P. D.: A high-accuracy map of global terrain elevations, *Geophys. Res. Lett.*, 44, 5844–5853, doi:10.1002/2017GL072874,
768 2017.

769 Yasuda, T. and Furuya, M.: Dynamics of surge-type glaciers in West Kunlun Shan, Northwestern Tibet, *J. Geophys. Res.*
770 *Earth Surf.*, 120, 2393–2405, doi:10.1002/2015JF003511, 2015.

771 Zhou, S., Yao, X., Zhang, D., Zhang, Y., Liu, S., and Min, Y.: Remote Sensing Monitoring of Advancing and Surging Glaciers
772 in the Tien Shan, 1990–2019, *Remote Sens.*, 13, 1973, doi:10.3390/rs13101973, 2021.

773 Zhou, Y., Li, Z., and Li, J.: Slight glacier mass loss in the Karakoram region during the 1970s to 2000 revealed by KH-9
774 images and SRTM DEM, *J. Glaciol.*, 63, 331–342, doi:10.1017/jog.2016.142, 2017.
775 Zhou, Y., Li, Z., Li, J., Zhao, R., and Ding, X.: Glacier mass balance in the Qinghai–Tibet Plateau and its surroundings from
776 the mid-1970s to 2000 based on Hexagon KH-9 and SRTM DEMs, *Remote Sens. Environ.*, 210, 96–112,
777 doi:10.1016/j.rse.2018.03.020, 2018.

778 Tables and Figures

779 **Table 1: Criteria for identifying surging glaciers based on changes in elevation and morphological features.**

<u>Surging feature</u>	<u>Identified class</u>	<u>Description</u>
<u>Elevation change</u>	<u>I-a</u>	<u>obvious thickening in lower reaches (e.g., ±30m)</u>
	<u>I-b</u>	<u>contrasting upper-thinning and lower-thickening (e.g., ±20m)</u>
	<u>I-c</u>	<u>contrasting upper-thickening and lower-thinning (e.g., +20m and -30m)</u>
	<u>I-d</u>	<u>severe thinning in the lower reaches (e.g., two times stronger than normal glaciers)</u>
	<u>II-e</u>	<u>moderate upper thinning and lower thickening (e.g., ±15m)</u>
	<u>II-f</u>	<u>only moderate thickening in the middle reaches (e.g., +15m)</u>
	<u>III-g</u>	<u>only moderate thickening at the terminus (e.g., +15m)</u>
	<u>III-h</u>	<u>only strong thinning in the lower reaches (e.g., one time stronger than normal glaciers)</u>
<u>Terminus advance</u>	<u>T1</u>	<u>strong terminus advancing (e.g., >500m)</u>
	<u>T2</u>	<u>slight terminus advancing (e.g., 0~500m)</u>
<u>Moraine change</u>	<u>M1</u>	<u>fast change of the looped moraine, or obvious distortion of the medial moraine</u>
	<u>M2</u>	<u>slow shape change of the looped moraine, or slight distortion of the medial moraine</u>

780

781 **Table 2: Surging glacier identification results.**

<u>Glacier changes</u>	<u>Identification class</u>			<u>Total</u>
	<u>I/T1/M1</u>	<u>II/T2/M2</u>	<u>III</u>	
2000-2020 elevation change	719	157	169	1045
1970s-2000 elevation change	507	156	57	720
1986-2021 terminus advance	247	397	-	645
1986-2021 looped moraine	112	31	-	144
1986-2021 medial moraine	69	29	-	108
Final identified surging glaciers	890 (verified)	208 (probable)	128 (possible)	1226

782

783 **Table 23: Results of surging glacier identification in 22 subregions of HMA. Only glaciers larger than 0.4 km² were considered in**
784 **the glacier number related values.**

<u>HiMAP regions</u>	<u>Glacier Number</u>				<u>Glacier Area</u>			
	<u>Surging</u>	<u>Surge-like</u>	<u>Total</u>	<u>Ratio* (%)</u>	<u>Surging</u>	<u>Surge-like</u>	<u>Total</u>	<u>Ratio* (%)</u>
Karakoram	354	128	4121	8.59	7936.12	1329.40	20103.68	39.48
Western Pamir	188	48	3058	6.15	2232.52	289.597	8172.64	27.32
Western Kunlun Shan	82	47	2508	3.27	2580.21	589.17	8466.12	30.48
Central Tien Shan	59	20	2248	2.62	881.61	305.47	6816.95	12.93
Eastern Pamir	56	16	1148	4.88	796.35	79.12	2746.47	29.00
Tanggula Shan	22	4	697	3.16	441.94	41.71	1937.39	22.81

Tibetan Interior Mountains	22	12	1471	1.50	286.29	140.22	3933.48	7.28
Northern Western Tien Shan	21	6	1374	1.53	116.27	81.09	2502.60	4.65
Central Himalaya	17	21	3433	0.50	164.12	185.07	9928.72	1.65
Eastern Kunlun Shan	16	7	1191	1.34	458.11	55.38	2960.26	15.48
Nyainqentanglha	10	5	2916	0.34	119.53	184.79	7216.62	1.66
Eastern Hindu Kush	9	5	1279	0.70	178.18	77.19	3055.80	5.83
Western Himalaya	9	4	3659	0.25	110.22	69.41	8619.19	1.28
Eastern Himalaya	6	0	1334	0.45	94	0	3371.89	2.79
Pamir Alay	5	0	991	0.50	35.72	0	1957.94	1.82
Qilian Shan	4	6	851	0.47	35.99	26.40	1627.94	2.21
Eastern Tibetan Mountains	3	2	156	1.92	36.33	3.85	341.46	10.64
Altun Shan	2	3	156	1.28	4.13	3.17	294.95	1.40
Eastern Tien Shan	2	1	1243	0.16	12.03	2.59	2440.11	0.49
Hengduan Shan	2	0	700	0.29	26.22	0	1335.39	1.96
Gangdise Mountains	1	0	768	0.13	10.52	0	1339.54	0.79
Dzhungarsky Alatau	0	1	407	0	0	10.98	648.61	0
Total	890	336	35709	2.49	16556.42	3474.60	99817.72	16.59

785 * The value of ratio only considered the number and area of verified surging glaciers.

786

787 **Table 34: The number and area ratios of surging glaciers in all glaciers for different area classes.**

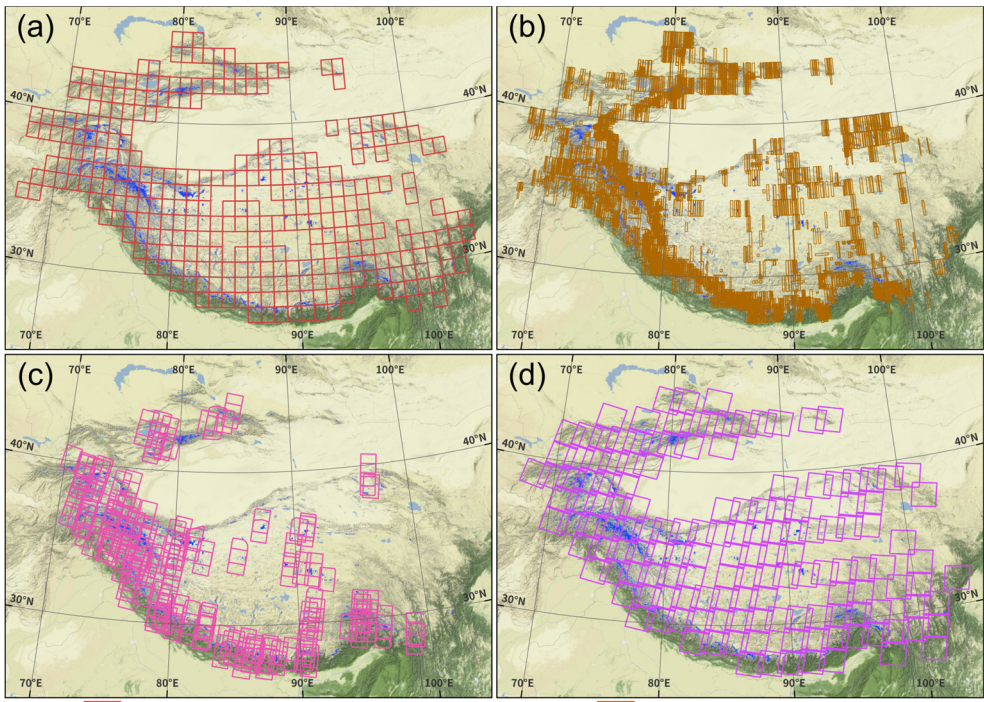
Area Class	Total		Surging Glacier		Ratio (%)	
	Count	Area (km ²)	Count	Area (km ²)	Count	Area
0.4-1	19428	12215.4	28	20.8	0.14	0.17
1-3	10983	18305.7	169	345.0	1.54	1.88
3-5	2404	9229.4	141	560.3	5.87	6.07
5-10	1650	11370.1	195	1416.4	11.82	12.46
10-30	946	15048.9	227	3861.2	24.00	25.66
30-50	161	5979.1	56	2036.5	34.78	34.06
50-100	92	6337.4	48	3329.2	52.17	52.53
100-300	39	6191.4	24	3651.5	61.54	58.98
>300	6	3466.3	2	1335.6	33.33	38.53

788

789 **Table 45: Attribute information in the present surging glacier inventory.**

Attribute	Description	Attribute	Description
Glac_ID	Glacier identifier composed by Lat/Lon	Surge_20	Surge identified in 2000-2020 by dH
Area	Glacier area (km ²)	Surge_70s	Surge identified in 1970s-2000 by dH
Zmin	Minimum elevation of the glacier (m a.s.l)	Delta_T	Identified class of glacier terminus advance
Zmax	Maximum elevation of the glacier (m a.s.l)	Loop_M	Identified class of looped moraine change
Zmed	Median elevation of the glacier (m a.s.l)	Medial_M	Identified class of medial moraine change
Slope	Mean glacier surface slope (°)	False_signal	False positive signal of identification
Aspect	Mean glacier aspect/orientation (°)	Trib_surge	If the glacier has/is surging tributary
MaxL	Maximum length of glacier flow line (m)	Surge_class	Final surge identification during 1970s-2020
HiMAP_region	HMA subregion that the glacier belongs to		

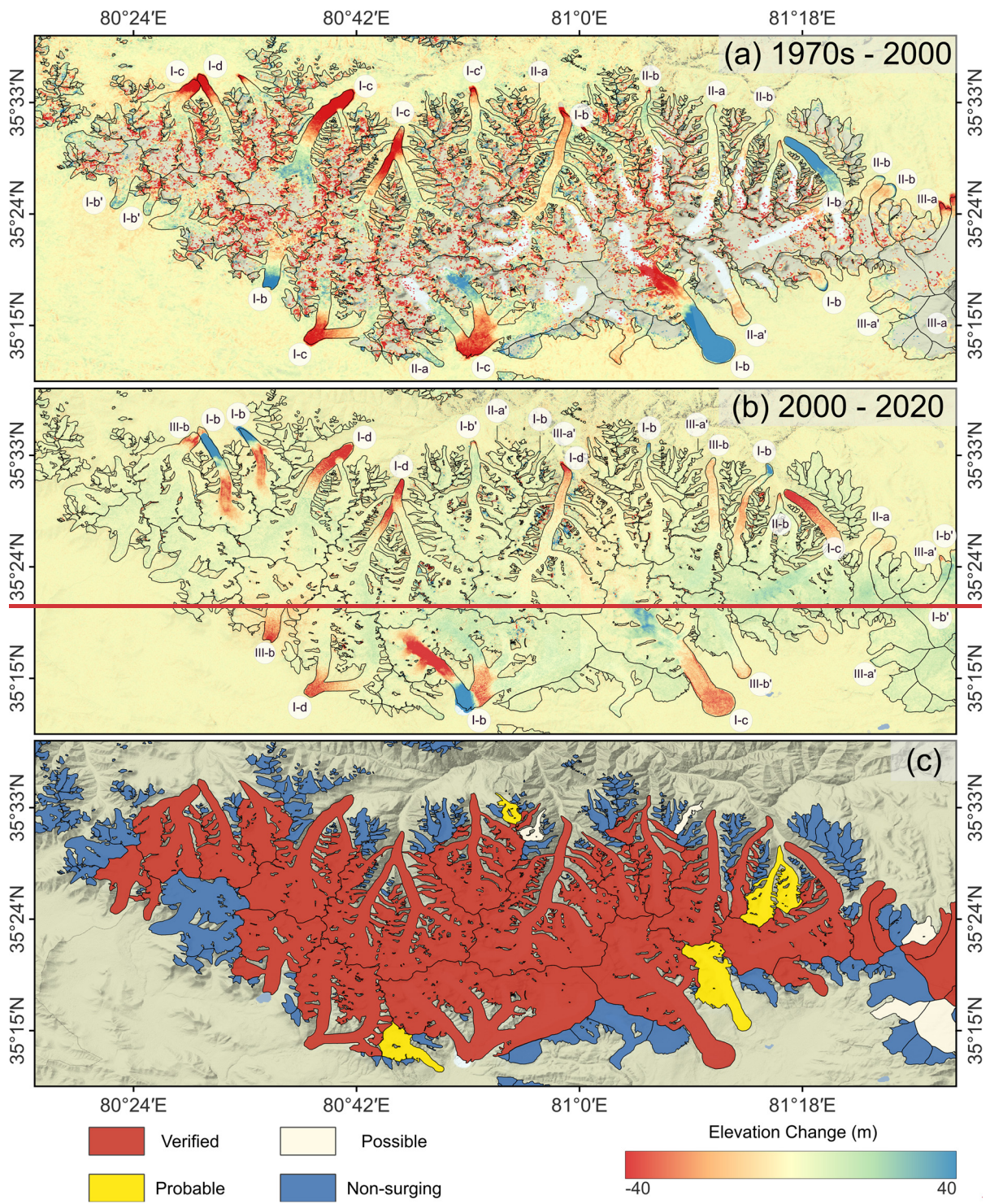
790



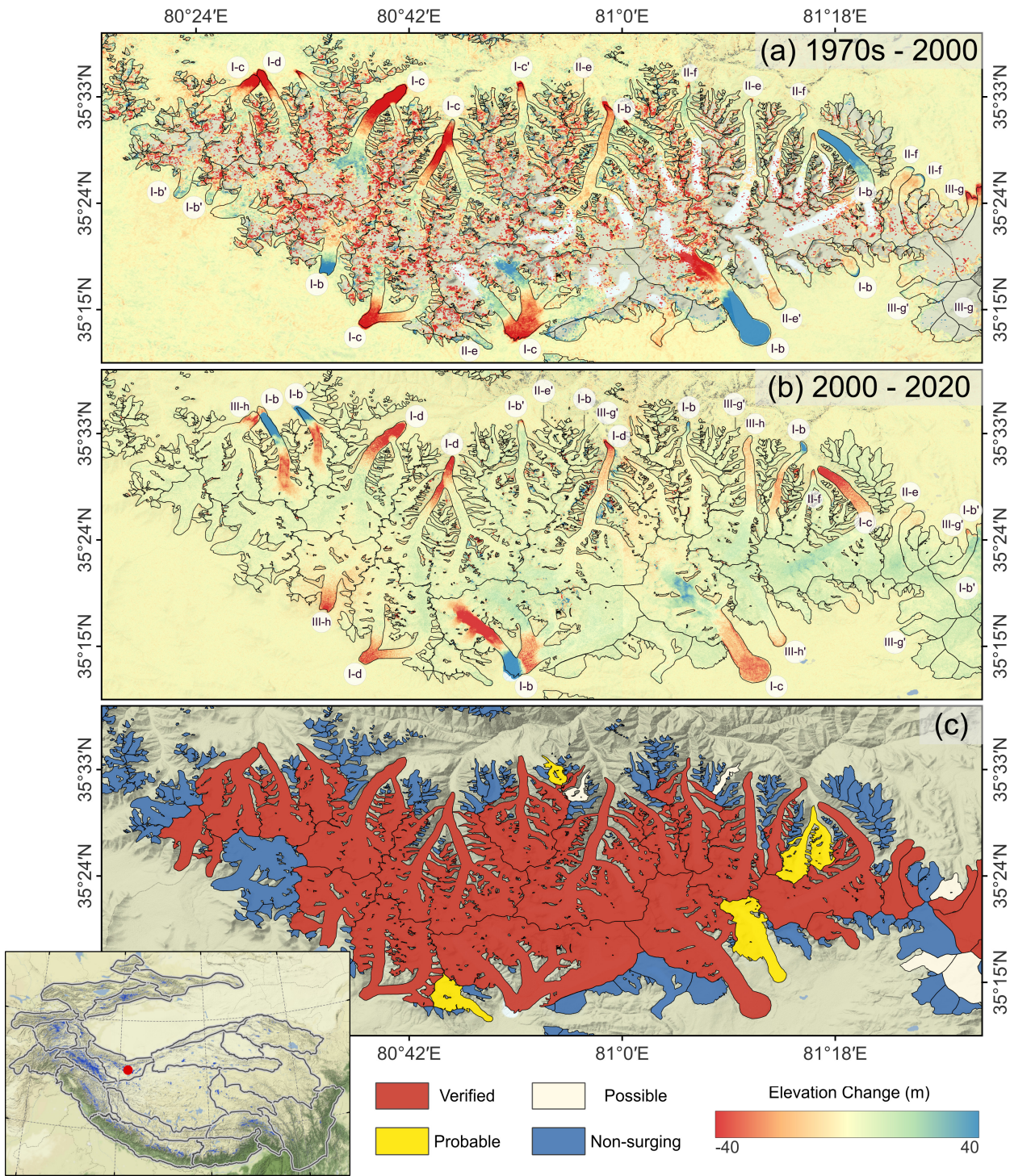
□ COP30 DEM/NASA DEM Footprint (313 tiles) □ HMA DEM Footprint (3598 tiles)
□ KH-9 DEM Footprint (238 tiles) □ Landsat images Footprint (148 frames)

791
792
793
794

Figure 1: Footprints of (a) the COP30/NASA DEMs, (b) the HMA DEMs, (c) the KH-9 DEMs, and (d) Landsat imageries that were utilized in this study. The background is rendered from the ESRI World Physical base map (Source: US National Park Service).



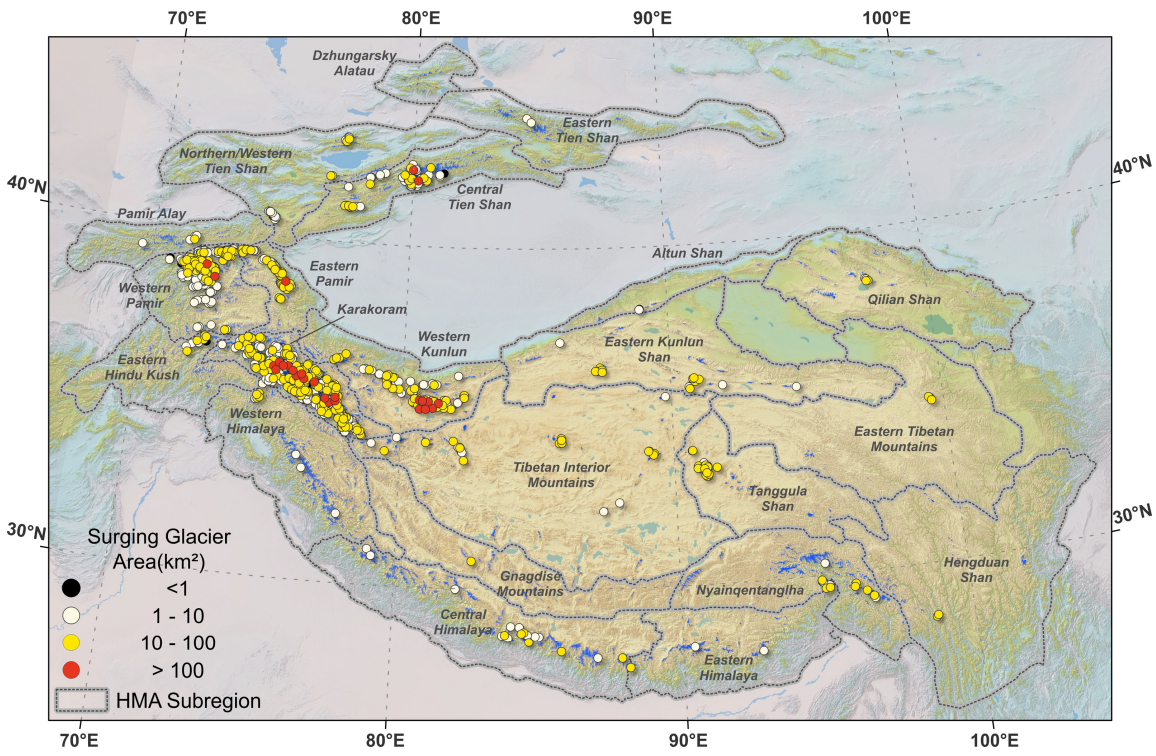
795



796

797 **Figure 2: An example of derived elevation change maps during (a) 1970s-2000, (b) 2000-2020, and (c) the surging glacier**
 798 **identification results. Black curves are glacier outlines. The labels in panels (a) and (b) represent the identified classes based on the**
 799 **elevation change patterns (the criteria of identification isare elaborated in section 4.2.1 and Table 1). The subscript “’” in the labels**
 800 **indicates that the surging glacier is identified by combining other elevation change maps. The red circle in the inset panel denotes**
 801 **the location of the area in the main panel (Western Kunlun Shan).** The background is the shaded relief of the COP30 DEM (Source:
 802 **ESA). The area is in the main massif of Western Kunlun Shan.**

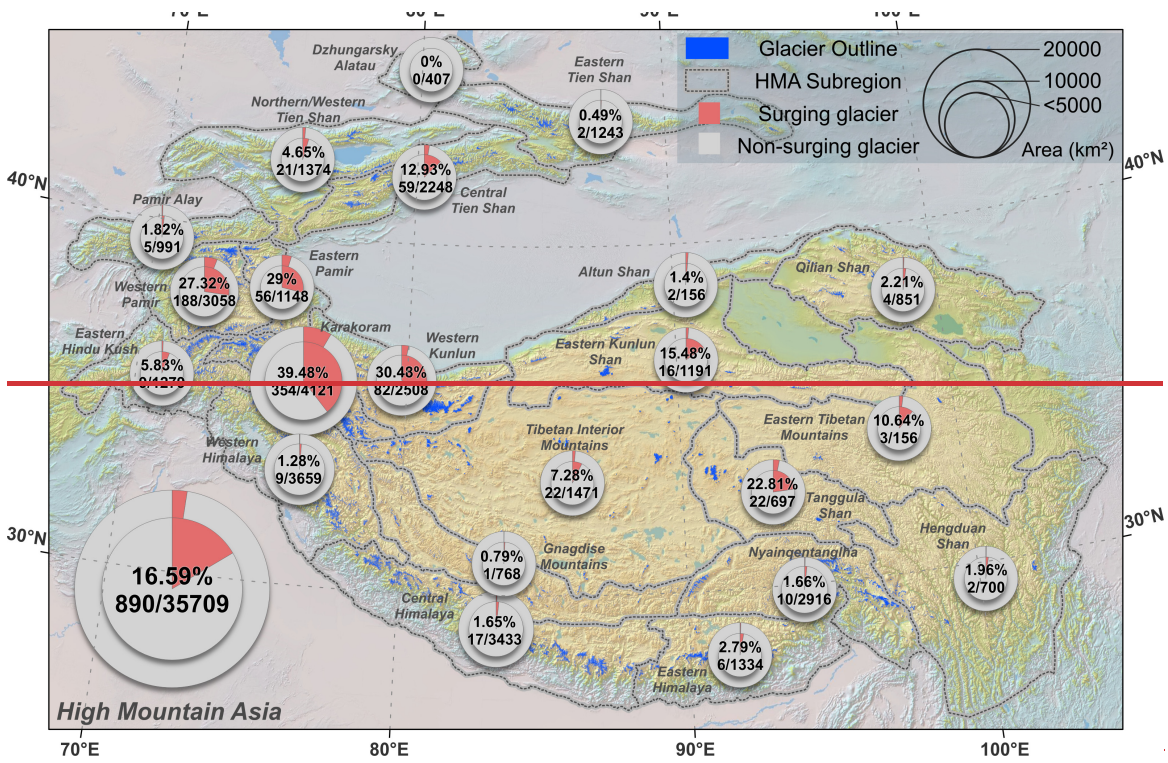
803



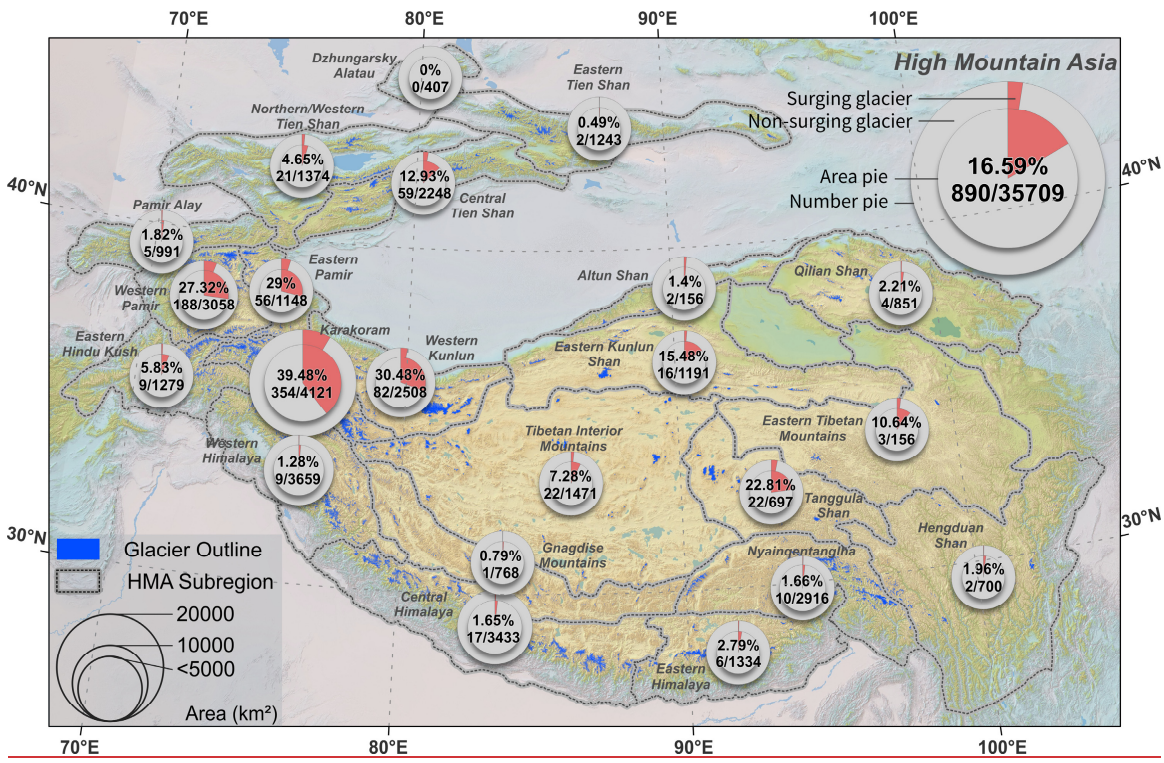
804

805 **Figure 3: Overview of the distribution of identified surging glaciers in 22 subregions of HMA. The background is the shaded relief**
 806 **of SRTM DEM (Source: USGS).**

807

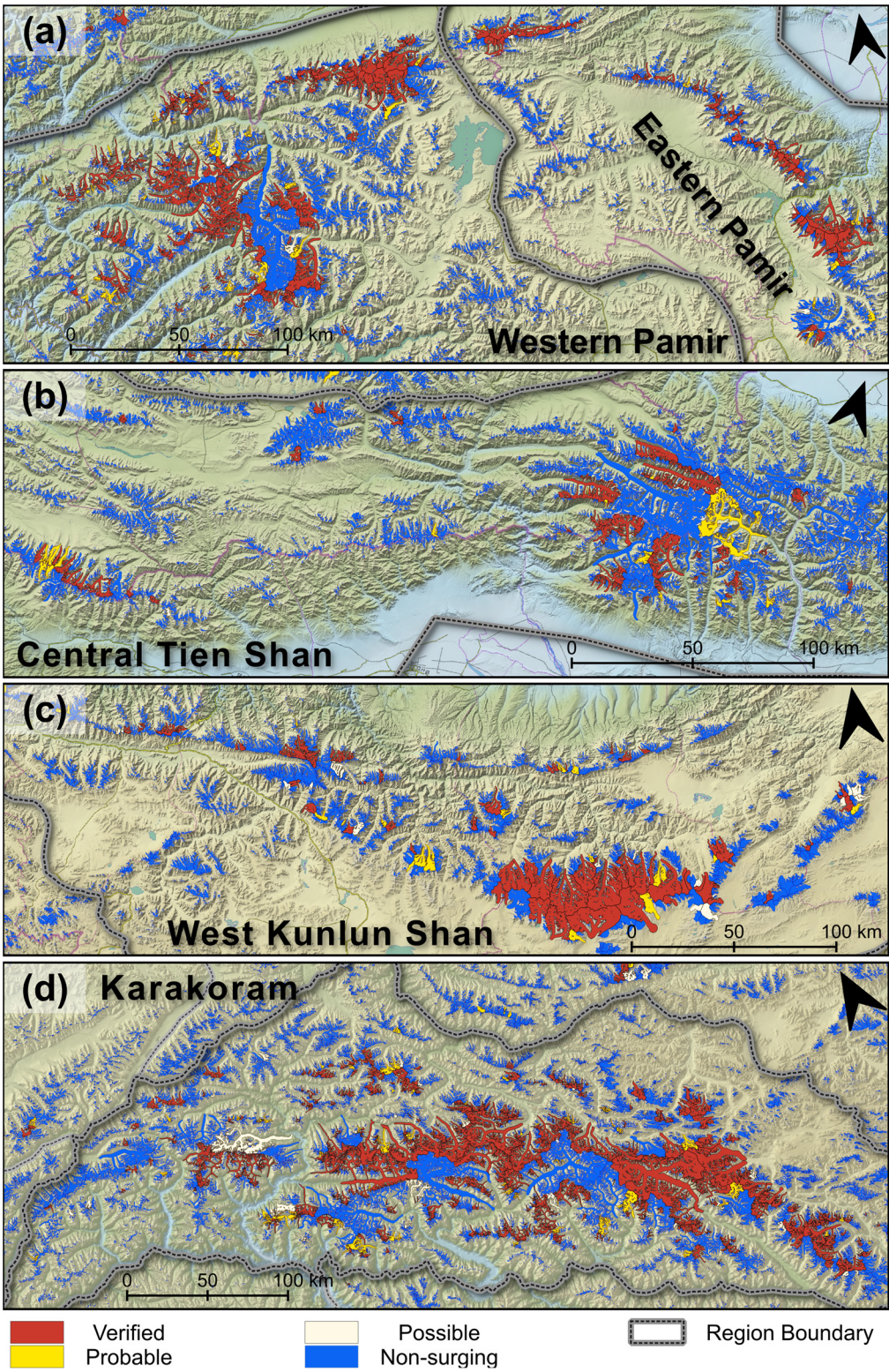


808



809

810 **Figure 4: Distribution of surging glaciers in the 22 subregions of HMA. The double-level pie chart represents the ratios of surging**
 811 **glacier number and area in each subregion. The inner pie denotes the area ratio labeled by a percentage, and the outer pie denotes**
 812 **the number ratio labeled by a fraction (only glaciers larger than 0.4 km² are considered). The background is the shaded relief of**
 813 **SRTM DEM (Source: USGS).**



814

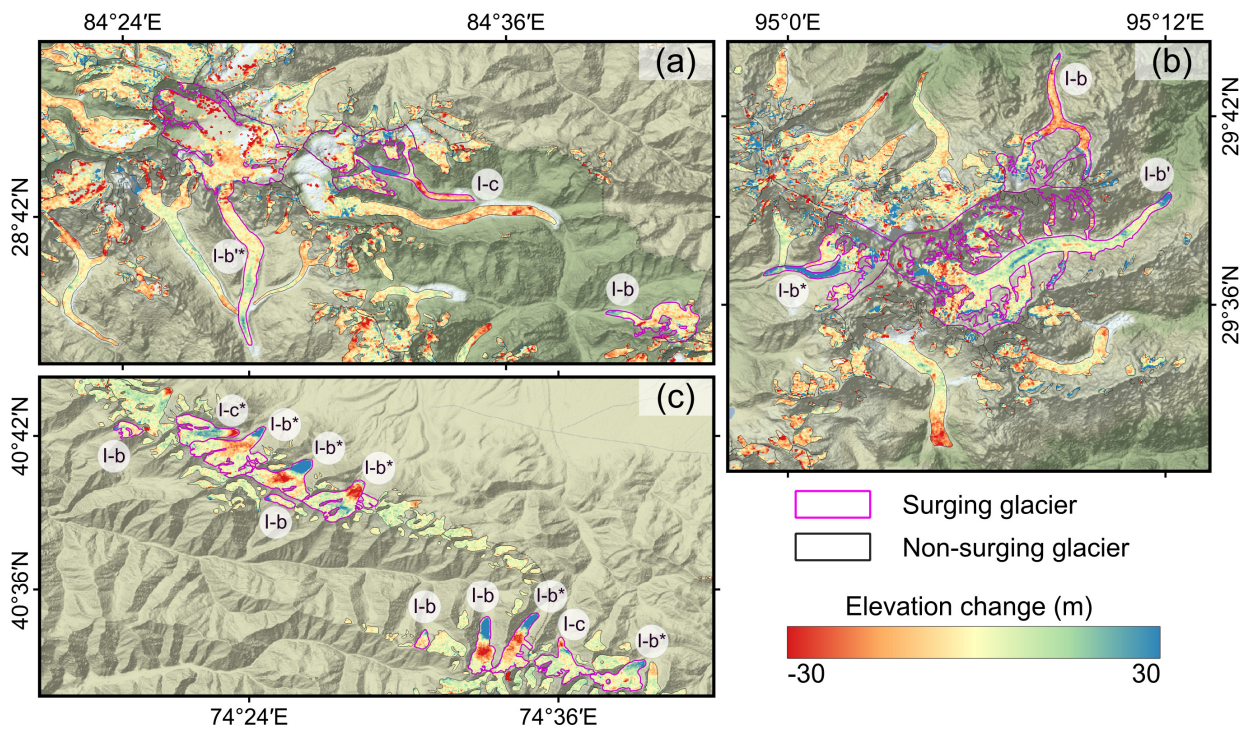
815

816

817

818

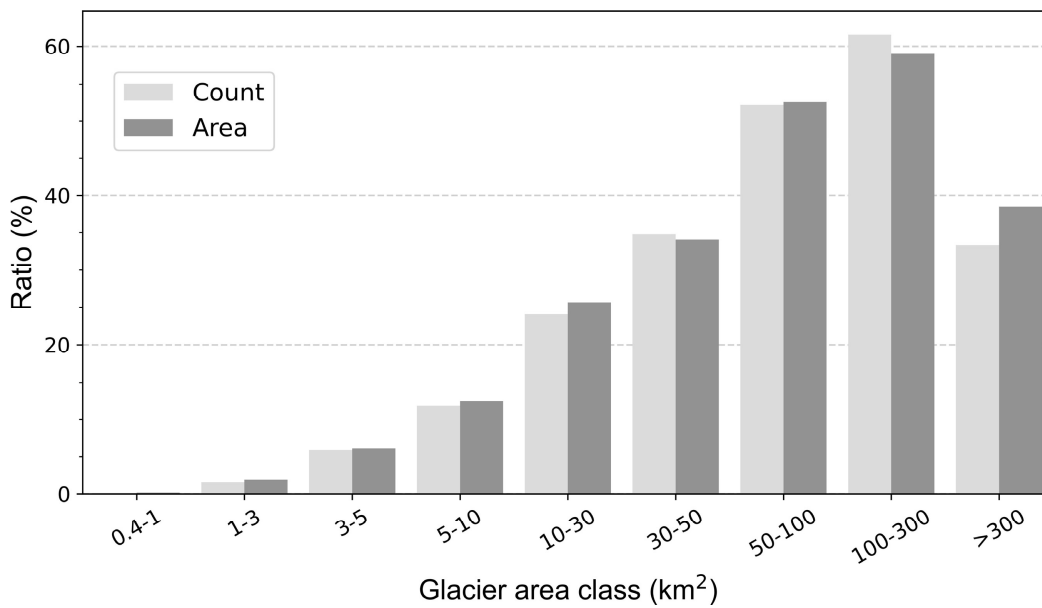
Figure 5: Results of surging glacier identification in (a) the Pamirs, (b) Central Tien Shan, (c) West Kunlun Shan, and (d) Karakoram. The background is the shaded relief of SRTM DEM (Source: USGS).



819

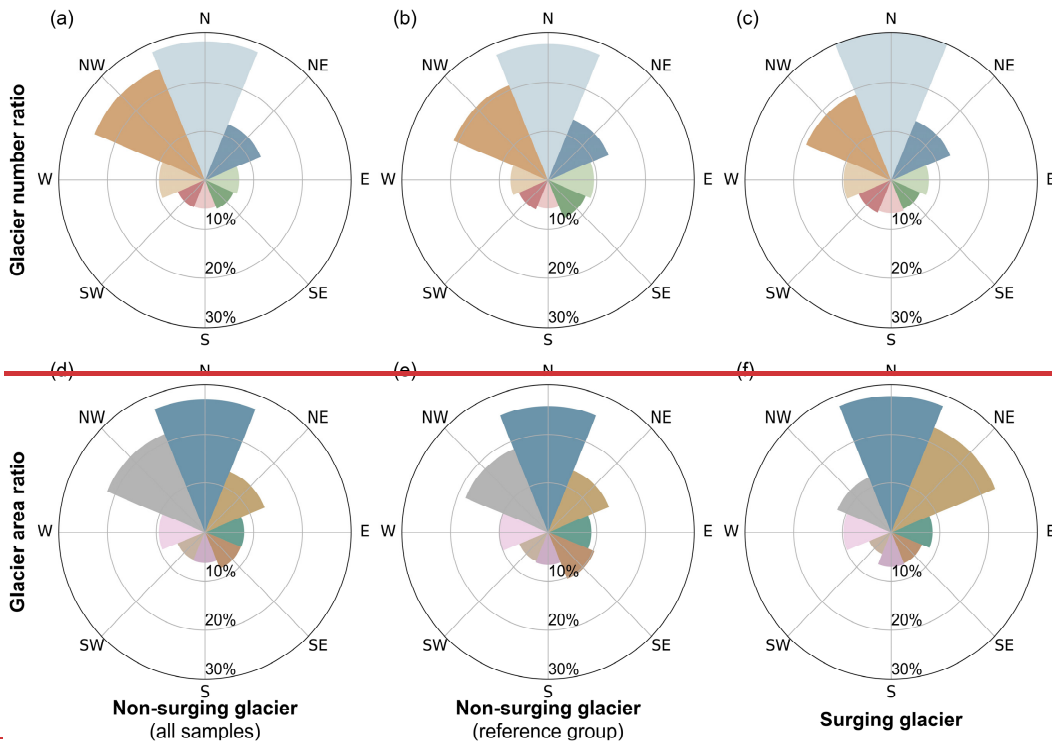
820 **Figure 6: Elevation change map of identified surging glaciers samples in (a) Central Himalaya (1970s-2000), (b) Nyainqentanglha**
 821 **(1970s-2000), and (c) Northern Western Tien Shan (2000-2020). The labels in panels (a) and (b) represent the identified classes based**
 822 **on the elevation change pattern- (the criteria of identification are elaborated in section 4.2.1 and Table 1). The subscripts ‘*’ and ‘’**
 823 **indicate that the identified class of the glacier is determined by combining morphological changes, and other elevation change maps,**
 824 **respectively. The background is the shaded relief of SRTM DEM (Source: USGS).**

825



826

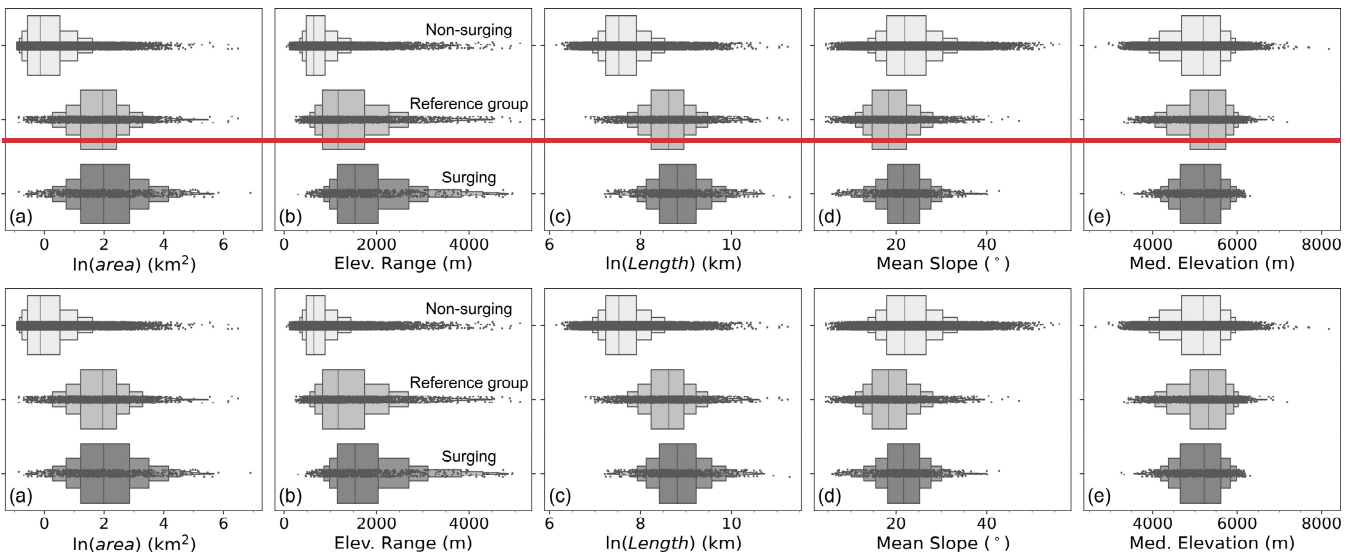
827 **Figure 7: Illustration of the number and area ratios of surging glaciers for different area classes.**



828

829 **Figure 8:** The distribution of glacier number and area in eight aspect sectors. Left column (a) and (d): distribution of glacier number
 830 and area ratio for non-surging glaciers; central column (b) and (e): distribution of glacier number and area ratio for non-surging
 831 glaciers in the reference group; right column (c) and (f): distribution of glacier number and area ratio for all surging glaciers.
 832 **Glaciers smaller than 0.4 km² were excluded from the non-surging glacier class.**

833

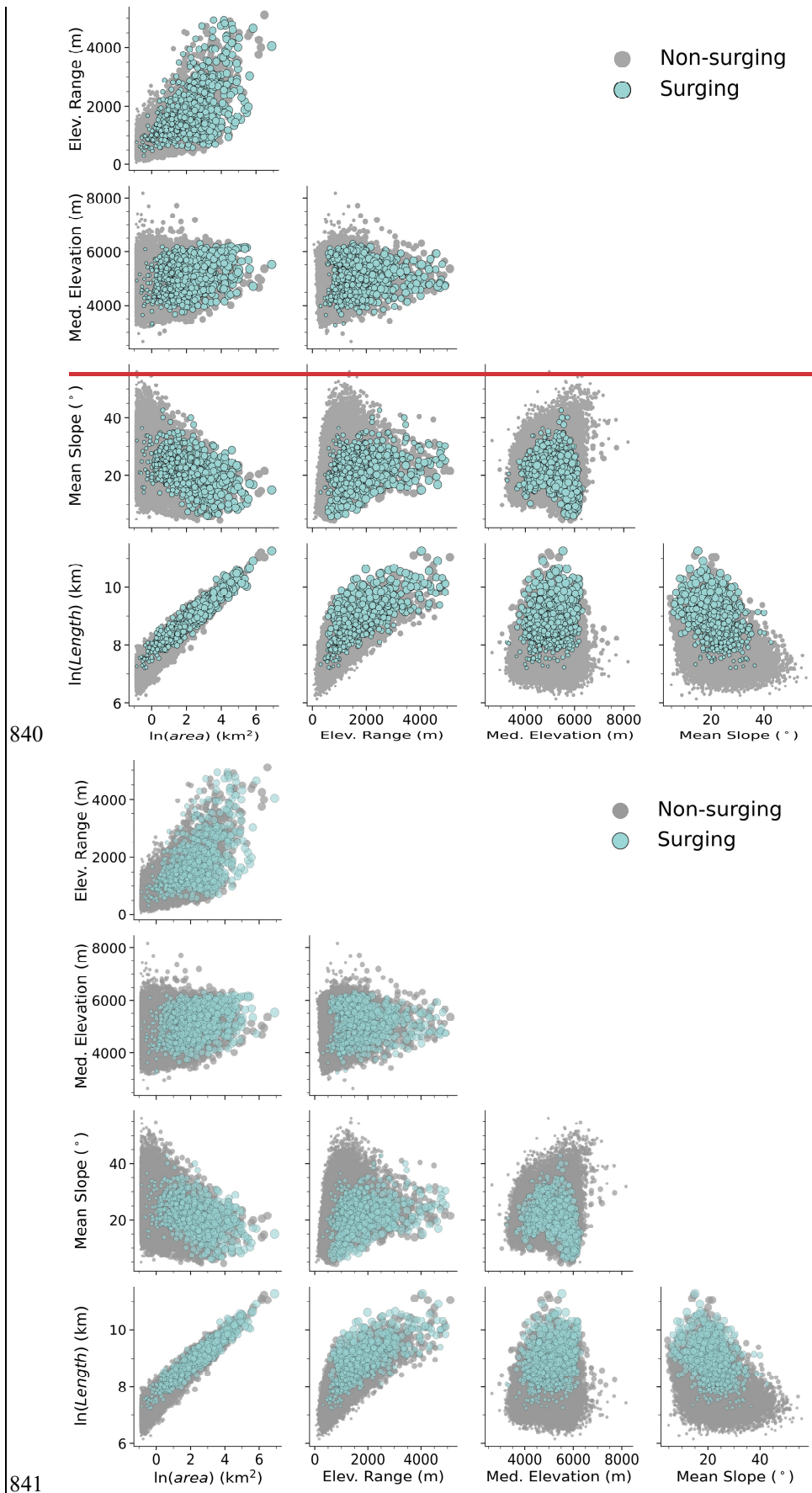


834

835

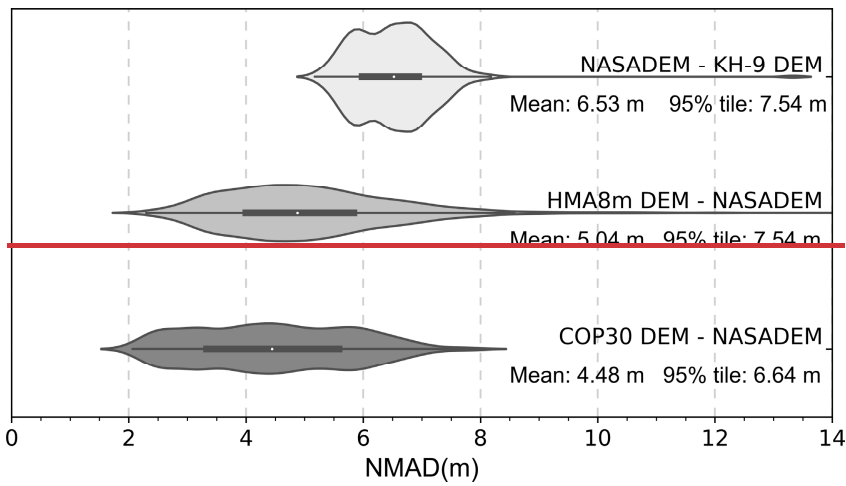
836 **Figure 98:** The comparison between the boxplots of geometric properties of non-surging glaciers (top), non-surging glaciers in the
 837 reference group (center), and surging glaciers (bottom). (a) Natural logarithm of area, (b) elevation range, (c) Natural logarithm of
 838 length, (d) Mean surface slope, (e) Median elevation. **Glaciers smaller than 0.4 km² were excluded from the non-surging glacier class.**

839

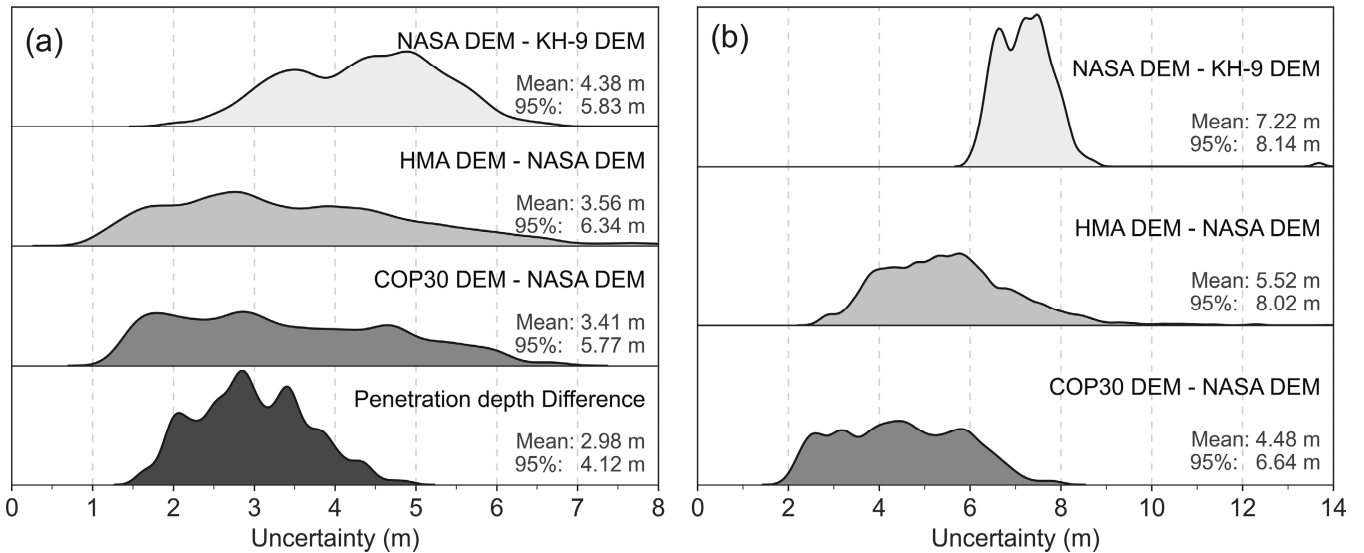


842 **Figure 109:** Bivariate scatterplots of geometric properties of non-surgingly and surging glaciers. The larger dots represent larger
 843 glaciers. Glaciers smaller than 0.4 km² were excluded in the non-surgingly glacier class.

844



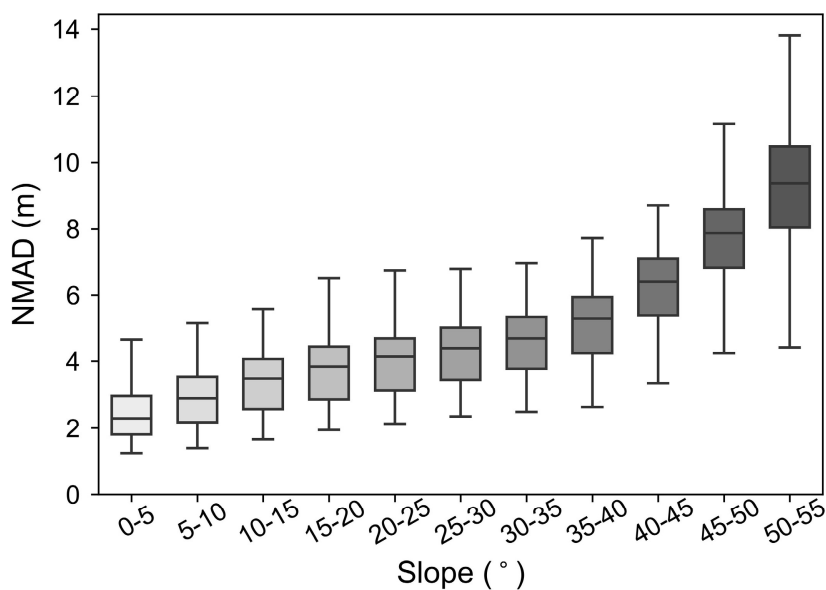
845



846

847 **Figure 110: The distribution of NMAD uncertainties in (a) four kinds of elevation difference observations and (b) three kinds of**
 848 **glacier elevation change observations in stable areas of all DEM differencing tiles. In each category, the shaded area denotes the**
 849 **density distribution of the uncertainties in corresponding observations the NMAD of all DEM differencing tiles. The white dot**
 850 **denotes the median in each group. The thick line represents the interquartile range (IQR, i.e., 75th percentile-25th percentile) in**
 851 **each group. The thin line represents the range between the minimum value (25th percentile - 1.5IQR) and the maximum value (75th**
 852 **percentile + 1.5IQR).**

853



854

855 **Figure 11: The distribution of NMAD of COP30 DEM – NASA DEM difference over stable regions within different slope ranges.**
 856 **The box denotes the interquartile range (IQR, i.e., 75th percentile-25th percentile) in each group. The horizontal line in the box**

857 denotes the median value in each group. The upper and lower line represents the range between the minimum value (25th percentile
858 - 1.5IQR) and the maximum value (75th percentile + 1.5IQR).
859